JGR Solid Earth

RESEARCH ARTICLE
10.1029/2021JB022904

Special Section:
Machine learning for Solid Earth observation, modeling and understanding

A Machine Learning-Based Approach to Clinopyroxene Thermobarometry: Model Optimization and Distribution for Use in Earth Sciences

C. Jorgenson[1], O. Higgins[1], M. Petrelli[2], F. Bégué[1], and L. Caricchi[1]

[1]Department of Earth Sciences, University of Geneva, Geneva, Switzerland, [2]Department of Physics and Geology, University of Perugia, Perugia, Italy

Key Points:

- Random forest machine learning is a novel approach for clinopyroxene thermobarometry with a comparable error to thermodynamic thermobarometers
- Model optimization was performed, and model performance is insensitive to most hyperparameters
- A detailed description of how to access and use the model is included so readers can use the thermobarometer

Supporting Information:

Supporting Information may be found in the online version of this article.

Correspondence to:

C. Jorgenson,
corin.jorgenson@unige.ch

Citation:

Jorgenson, C., Higgins, O., Petrelli, M., Bégué, F., & Caricchi, L. (2022). A machine learning-based approach to clinopyroxene thermobarometry: Model optimization and distribution for use in Earth sciences. *Journal of Geophysical Research: Solid Earth*, *127*, e2021JB022904. https://doi.org/10.1029/2021JB022904

Received 11 AUG 2021
Accepted 22 MAR 2022

Author Contributions:

Conceptualization: C. Jorgenson, O. Higgins, M. Petrelli, L. Caricchi
Methodology: C. Jorgenson, O. Higgins, F. Bégué, L. Caricchi
Supervision: M. Petrelli, L. Caricchi
Writing – original draft: C. Jorgenson, O. Higgins

Abstract Thermobarometry is a fundamental tool to quantitatively interrogate magma plumbing systems and broaden our appreciation of volcanic processes. Developments in random forest-based machine learning lend themselves to a data-driven approach to clinopyroxene thermobarometry, allowing users to access large experimental data sets that can be tailored to individual applications in Earth Sciences. We present a methodological assessment of random forest thermobarometry using the R freeware package `extraTrees`. We investigate the model performance, the effect of hyperparameter tuning, and assess different methods for calculating uncertainties. Deviating from the default hyperparameters used in the `extraTrees` package results in little difference in overall model performance (<0.2 kbar and <3°C difference in standard error estimate, SEE). However, accuracy is greatly affected by how the final value from the distribution of trees in the random forest is selected (mean, median, or mode). Using the mean value leads to higher residuals between experimental and predicted P and T, whereas using median values produces smaller residuals. Additionally, this work provides two scripts for users to apply the methodology to natural data sets. The first script permits modification and filtering of the model calibration data set. The second script contains premade models, where users can rapidly input their data to recover PT estimates (SEE clinopyroxene-only model: 3.2 kbar, 72.5°C and liquid-clinopyroxene model: 2.7 kbar, 44.9°C). Additionally, the scripts allow the user to estimate the uncertainty for each analysis, which in some cases is significantly smaller than the reported SEE. These scripts are open source and can be accessed at https://github.com/corinjorgenson/RandomForest-cpx-thermobarometer.

Plain Language Summary Determining the structure of magmatic plumbing systems is an integral part of understanding the processes preceding volcanic eruptions. Thermobarometry estimates the pressure and temperature of crystallization of minerals using their chemical composition. These minerals are erupted to the surface in magma during eruptions (melt plus crystals). This can provide quantitative information on the depth and temperature of magma storage before eruption. Clinopyroxene, a common crystal found in volcanic rocks, has been shown to be a reliable mineral for thermobarometry. Commonly, thermobarometers use a single equation for a specific melt chemistry and are often rigid in their usage. There exists an alternative methodology, which utilizes a machine learning algorithm called random forest. This algorithm creates hundreds of hierarchical flowcharts called decision trees to generate predictive models, which can be applied to natural data. Here, we present a study that focuses on optimization of these models and presents users with two versions, which they can access, modify, and use for their data. These two versions are available freely at https://github.com/corinjorgenson/RandomForest-cpx-thermobarometer and can be easily used within the freeware package R.

1. Introduction

Quantifying the pressure and temperature of mineral crystallization is an invaluable method to retrieve information on architecture of volcanic plumbing system of volcanoes and constrain magma migration and storage through the lithosphere (Giacomoni et al., 2016; Ridolfi et al., 2008; Shane & Smith, 2013; Shaw, 2018a; Smith, 2013). Clinopyroxene chemistry has been widely used for this endeavor by calibrating thermobarometers (Masotta et al., 2013; Neave & Putirka, 2017; Putirka, 2008; Wang et al., 2021). Classically, these thermobarometers result in a single equation, which links site-specific mineral chemistry (plus or minus equilibrium liquid data) to the variation in pressure or temperature of crystallization. However, these formulas are often associated with large standard error estimates (SEE) and are only appropriate for specific melt compositions (e.g., Neave &

Writing – review & editing: O. Higgins, M. Petrelli, F. Bégué, L. Caricchi

Putirka, 2017 for ultramafic to intermediate compositions; Masotta et al. (2013) for alkaline magmas). Additionally, early thermobarometer calibrations were self-validated, which means that data used to regress the model are also used to validate it. This typically leads to data overfitting and an underestimated SEE (Nimis & Taylor, 2000; Putirka, 2008). Recent developments in machine learning applications to petrology by Petrelli et al. (2020) and Higgins et al. (2022) have resulted in a machine learning random forest approach to thermobarometry. Both studies omitted several pertinent experimental data sets of clinopyroxene and liquid equilibria, which are now included in the model presented here.

Random forest is a machine learning method that employs decision trees to populate an improved prediction-based model, using the results from a distribution of hundreds of trees to generate an output (Breiman, 2001, 2002; Ho, 1995). A decision tree is a hierarchical flowchart that determines an outcome when given a set of input variables (Figure 1). Each tree is composed of branches and leaves, where the branches represent different pathways from the root to the desired outcome (the leaves). Branches split at nodes, where at each node, a branch may spilt either left or right in the simplest case. When a branch can no longer split, a leaf is "grown," and the desired output is reported. In our case, the branches and nodes are dictated by clinopyroxene geochemistry, and the leaves are pressure (P) or temperature (T) of crystallization. However, the chemical element (or oxide) selected at each node greatly influences the predictive outcome of the tree. Hence, the random forest model is composed of hundreds of decision trees. Therefore, from these hundreds of decision trees, the output (predicted P or T) is the mean value from all decision trees in the case of regressive models. To allow the model to construct reasonable decision trees for prediction of natural data, we input a data set of experimentally derived clinopyroxenes (e.g., Figure S1 in Supporting Information S1) with a known pressure and temperature of crystallization, hereafter referred to as the calibration data set. In principle, the idea is very simple—the algorithm uses the calibration data set to create a predictive model, which we can apply to natural samples. However, there are several parameters to consider when calibrating a model for reliable prediction of natural data, in addition to several statistical metrics for selecting the best estimation from the voting distribution of decision trees (e.g., mean, median, or mode). Importantly, the performance of the algorithm is assessed using experiments that were not included in the calibration data set. This is done by extracting a testing data set from the initial data set that does not see the model prior to testing. This process is repeated 200 times for statistical significance and allows all the data of the data set to be used without using self-validating methods.

Increasingly, models and methodologies for Earth science applications have moved to powerful and adaptable codes for programs such as R, python, and MATLAB as well as hosted on online servers, such as github (Georgeais et al., 2021; Ghiorso & Wolf, 2019; Iacovino et al., 2020; Lemenkova, 2019; Lubbers et al., 2019). This allows for more user interaction and in some cases provides open-source options to users regardless of their operating system or access to apps like excel. Thus, the twofold aim of this work is to (a) build and test the performance of a thermobarometer model for clinopyroxenes and (b) provide a comprehensive explanation of how to apply our thermobarometer for applications to natural data. Our regression strategy offers a generalized model that can be tailored for certain settings, applications, or other suitable mineral phases (e.g., amphibole; Higgins et al., 2022). We greatly expand the data set of clinopyroxene and liquid equilibria in our calibration data set compared to previous studies, allowing our calibrations to be as globally applicable and adaptable as possible for users.

2. Methods

2.1. Data Sets and Preprocessing

The calibration data set is composed of experimentally grown clinopyroxenes and equilibrium liquids compiled from the Library of Experimental Petrology Research database and additional works not included in the LEPR database (Hirschmann et al. (2008); Table S1 in Supporting Information S1). The unfiltered calibration data set features 2571 datapoints, including temperatures from 679 to 2180°C, 0–160 kbar, and 6.5–78.18 wt.% SiO_2. Following the works of previous thermobarometers, we use an equilibrium filter on the basis of the Fe-Mg exchange, accepting only data within a 1 sd of the average $Kd_{Fe\text{-}Mg}$ of the unfiltered data set (Klügel & Klein, 2006; Putirka, 2008, 2016; Ziberna et al., 2016; Figure S1a in Supporting Information S1). This is a relatively stringent test but may be adapted by users within the script if preferred. The data were then filtered to remove the rare high-pressure experiments (>30 kbar) or low SiO_2 liquid contents (<35 wt. % SiO_2). These regions are removed as they are rare in the calibration data set and we find poorer performance from the model for regions of the

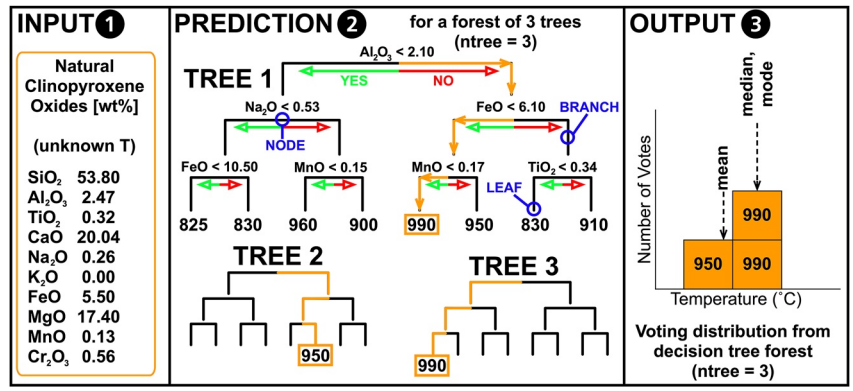

Figure 1. Process of determining temperature from a natural (unknown T) clinopyroxene using machine learning thermobarometry. The input to the model (1) is the chemistry of the natural clinopyroxene. The chemical composition is cascaded through each decision tree in turn (2; orange path), arriving at the temperature at the base of each tree. The voting distribution (3; output) is used to determine the temperature. This temperature can be selected based on the mean, median or mode of the voting distribution (see text for details).

calibration data set with sparse data due to the limited extrapolative ability of machine learning. This forms the final calibration data set (n = 2079, Table S1, Figure S1 in Supporting Information S1). The role of H_2O in the melt may also be an indicator of PT conditions, but as it is not consistently reported in the literature, we omit it from these models (Behrens et al., 2009; Ghiorso & Gualda, 2015; Newman & Lowenstern, 2002).

Typically, thermobarometers are calibrated and tested in the following way. First, a large (>80% of total experiments) training data set is selected from the total calibration data set of experiments. This data set is used to calibrate with the chosen regression strategy (e.g., linear regression and multivariate linear regression). The remaining data are placed into a test data set, which is used to assess the performance of the model. This is commonly achieved by running each composition in the test data set through the regressed model and calculating the standard error estimate or distribution of residual values to the known experimental values (Putirka, 1999, 2008; Ridolfi et al., 2008).

The pressure-temperature distribution of the calibration data set is not uniform—experiments are preferentially run at low pressures. Thus, randomly extracting from the calibration data set unevenly weights the test set to have low pressure experiments, resulting in a poor representation of the SEE. To circumvent this issue, our test data set was uniformly extracted from the calibration data set on a gridded basis (Figure S1b in Supporting Information S1). Sampling from a gridded distribution offers additional biases, such as oversampling PT grid spaces, that may have a small distribution of data (i.e., a grid may have only 1 out of the total 2079 points sampled)—thus, the grid spacing was randomized for each 200 runs and samples were not extracted if the grid space did not have at least two datapoints. This results in each test data set sampling approximately a tenth of the total calibration data set. Once the respective test and train data sets are extracted, then the model is run for each set (200 times). By generating multiple random splits of test and train data sets, we can evaluate the full effect of sampling on the SEE (and other model performance metrics). This effect is not considered in conventional calibration methods (e.g., Ridolfi et al., 2010; Ridolfi & Renzulli, 2012). This methodology has benefits over a weighted mean as it removes data with an inverse proportionality to the number of experiments performed at specific conditions, while not removing single experiments performed within a single element of our grid. We note that the calibration data set has pressure and temperature uncertainties associated with different experimental setups, for example, temperature gradients along a capsule. These errors, however, are sufficiently small when compared to the calibration SEE and thus are not propagated through the model. Finally, experiments performed at the highest pressures are also performed at the highest temperatures, which make experimental pressure and temperature not independent. This aspect should be considered especially when temperature is used as an input parameter to retrieve pressure information as it could lead to biased pressure estimates. In our model, we do not use temperature as an input parameter to estimate pressure.

2.2. Components of a Random Forest

We chose to use the package `extraTrees` developed by Simm et al. (2014) although the `randomForest` package by (Breiman, 2002) produces comparable results at greater computational expense (Petrelli et al., 2020). The `extraTrees` package includes several parameters that can affect model performance. First, `ntree` (default = 500) determines the number of individual decision trees, which are used for prediction. A sufficiently high number of trees must be used to provide stability of the variable importance. The number of trees should be considered a convergent variable, where beyond a certain threshold performance improvement is marginal and the number of trees should be minimized to save on computational time without sacrificing performance (Breiman, 2001; Probst & Boulesteix, 2018; Probst et al., 2019; Sage et al., 2020). Second, `mtry` dictates how many variables (in our case, the major element chemical constituents of clinopyroxene) are considered at each node. The `mtry` is more influential on the overall performance of the model and default `mtry` for `extraTrees` is the total number of variables divided by three (Probst et al., 2019; Simm et al., 2014). For each node in a decision tree, a random subset of variables equal to `mtry` are selected from which the best performing variable is eventually chosen. In `extraTrees`, each node is split at a random value as described (Simm et al., 2014). To choose which of the selected variables is used for the next node, a score is calculated for each variable for regressive models. This score is calculated considering a proportional negative variance for each split (denoted by L for left and R for right).

$$score = n_L * var_L + n_R * var_R \tag{1}$$

$$var = -\frac{1}{n}\sum_{i=1}^{n}(y_i - mean(y))^2 \tag{2}$$

where n_L and n_R are the number of datapoints assigned to each left or right branch, and var is the negative variance of the data on the left (or right) side of the split for the y variables (Simm et al., 2014). The tested variable with the highest score is chosen for the node (See Figure S2 in Supporting Information S1 for further explanation).

The `extraTrees` package provides an additional variable for modification, which is the number of random cuts (`numRandomCuts`; the number of branches at a given node) where greater than two splits is termed nonbinary splitting. As noted in the `extraTrees` vignette, optimization may occur when using `numRandomCuts` between 3 and 5. We found a minor improvement in the SEE (<0.02 kbar), but the increase in computational time negated any positive effects of more splits.

Each decision tree generates a single output value and thus a forest with 300 trees generates 300 pressure or temperature estimates. By default, in regression mode, random forest algorithms consider the mean or the mode values to return an estimate in regression or classification mode, respectively. In addition to the mean, we additionally calculate the median and modal estimates to evaluate the model performance. The median is calculated by taking the middle value from a sorted set of values. Thus, to avoid the rare case where there is an even number of trees, and the two center points are drastically different, we have decided to use an odd number of trees to average the two values.

2.3. Error Assessment

Before continuing, we must consider the argument of accuracy versus precision. Random forest is effective at generating precise values, but a reliable thermobarometer needs to be accurate as well as precise. As such, the evaluation of the uncertainty of an individual model based on R^2 values (Equation 3, where RSS is the residual sum of squares and TSS is the total sum of squares) and the residual values (absolute difference between the experimental temperature or pressure and the temperature or pressure output from the model), in addition to the standard error estimate (SEE) and the interquartile range (IQR) of the voting distribution.

$$R^2 = 1 - \frac{RSS}{TSS} \tag{3}$$

To avoid self-validation and overfitting, data within the test data set must not be used in the data set, which trains the model (training data set). Varying the test data set is one of the largest sources of variation in the SEE and so we resampled the calibration data set 200 times to produce 200 separate tests and training data sets. Then, the average SEE is taken from the distribution of errors for all 200 data set splits. Two hundred runs were chosen as this is

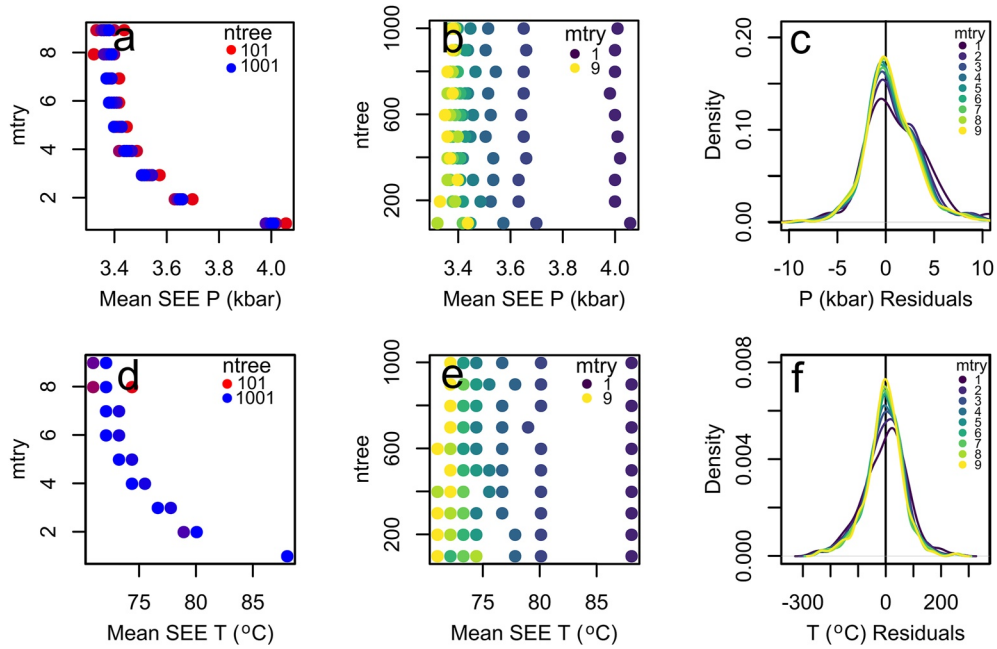

Figure 2. Distribution of the `mtry` (a and d), `ntree` (b and e), and residuals (c and f) for both pressure and temperatures calculated using the median method. Each point represents the SEE for one split of the training and testing data set for each `mtry` and `ntree` combination. The residual plots are density plots of the residuals for `mtry` values from 1 to 9, at a constant `ntree` of 200.

the minimum number of runs where the SEEs are normally distributed, thus preserving computational cost while maintaining a representative assessment. When the chemistry of the mineral under consideration is close to one of the analyses from the experiments, the distribution of estimates is characterized by low values of the IQR (which can be significantly smaller than the SEE). Therefore, we also use the IQR to calculate a confidence interval of each estimated value. We recommend users remove natural data estimates for which the IQR is double the models SEE as these are considered outside of the model error (e.g., for a model SEE of 3.4 kbar use an IQR filter of 6.8).

3. Results

3.1. Hyperparameter Tuning

Hyperparameter tuning aims to structure the best performing model possible (Breiman, 2002; Probst & Boulesteix, 2018). To systematically test the effect of hyperparameter variability, we ran 19,980 simulations, which encompass 90 combinations ranging from 1 to 9 `mtry` and 101–1001 `ntrees` where each permutation is run 200 times with the respective test and train data sets to determine the average SEE and R^2, calculated using the ideal median pressures and temperatures.

The mean SEE varies with the number of trees (Figure 2) where the smaller number of trees performs marginally worse than the larger number of trees (Figure 2b). This is because the number of trees is a convergent parameter as seen in other studies focused on hyperparameter tuning of random forests (Oshiro et al., 2012; Probst et al., 2019; Sage et al., 2020). Figure 2 (b, e) show a slight negative trend in both the pressure and temperature between 101 and 201 trees, but we stress that the difference is marginal. Clearly, we can see that the `mtry` has a larger control on the performance of the model as expected from results in previous studies (Probst et al., 2019; Simm et al., 2014). As seen in Figure 2 (a, d), the larger `mtry` performs better (e.g., at `ntree` = 201 and `mtry` of 6 gives a mean SEE of 3.13 kbar and 70°C) than the smaller `mtry` (e.g., at `ntree` = 201 `mtry` of 1 give a mean SEE of 3.77 kbar and 83°C) for both the mean SEE and residuals. At `mtry` greater than 6, any difference is minor (±0.01 kbar), and so to limit computational cost, an `mtry` of 6 should be used. This is counter to the package default, which is one third the number of total variables. A similar trend is observed in the calculated IQR. However, when considering data with the inclusion of liquid—crystal pairs, the new maximum `mtry` is 18 and hence a new `mtry` needs to be considered.

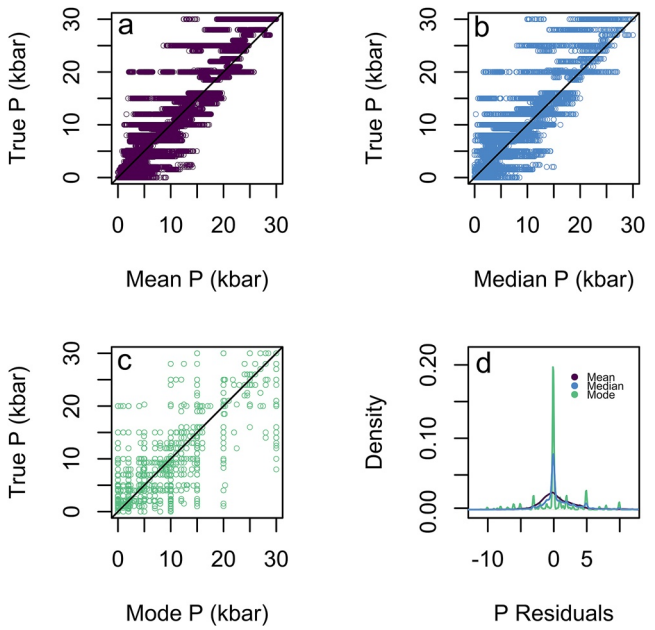

Figure 3. Mean (SEE = 3.20 kbar, $R^2 = 0.863$) (a), median (SEE = 3.3 kbar, $R^2 = 0.861$) (b), and modal (SEE = 4.0 kbar, $R^2 = 0.782$) (c) pressure determinations for the 200 test datasets versus their true pressure (44400 points plotted). (d) Density plots of the residuals for the mean, median, and mode. Here we see that the mean and median are similar in their estimates, but when the residuals are compared the median performs much better. The mode has a high concentration of points at 0 residuals but shows a many more poor residuals at higher values, thus the median is the best option to use to get the most accurate data.

We performed further testing on the model with the increased maximum `mtry` and found that although the computational time increased, the models followed the same pattern as clinopyroxene only models whereby performance is relatively insensitive to `ntree` value and the `mtry` is optimized at about two thirds of the total variables (Figure S3 in Supporting Information S1). As such, we suggest users to select an `ntree` of 201 and an `mtry` equal to two thirds of the total input variables, which are hyperparameters that will minimize the computational cost without sacrificing accuracy (clinopyroxene oxides in the case of thermobarometry).

The package `extraTrees` also provides the option to vary the number of cuts at each node. This is conceptualized in a classification model for grouping people on the basis of hair color: instead of discriminating between black or blonde hair (binary choice with 1 cut), brown hair and red hair can be considered as additional options (3 cuts). While the default is 1 cut (binary; two branches at a node), increasing the number of cuts to 3–5 may yield marginal performance improvements (Simm et al., 2014). Upon further testing, we found that the additional number of cuts from 1 to 2 does minorly improve the model. However, the minor improvement of the SEE is less than 0.02 kbar and 0.5°C and so is not worth the significant increases in computational cost (Figure S4 in Supporting Information S1). Therefore, we continue to use the default of 1 cut.

3.2. Mean, Mode, and Median Estimates

As previously discussed, the random forest is composed of several hundred decision trees as defined by the user via the function argument `ntree`. For each input sample, `ntree` estimates of pressure and temperature are generated, and the final value is chosen from this voting distribution. The default option of the R package `extraTrees` in regression is for the forest to choose the mean of all decision tree outputs as the final pressure or temperature (Simm et al., 2014). However, the distribution of the decision trees may not be a perfect Gaussian distribution and thus we have also considered the median and modal estimates of the pressure and temperature voting distributions in addition to the mean (Figure 3).

To evaluate the performance of the mean, median, and modal estimates, we create pressure and temperature models using the entire calibration data set for clinopyroxene. Figure 3 shows estimated pressure plotted with respect to the true pressures for all 200 test data splits, using the mean, median, and modal method. The residuals, the difference between the estimated and true pressure and temperature estimates, show the widest distribution of residuals for the mean, extending out to ±5 kbar, indicating a poorly performing model. When we consider the SEE, the median outperforms the mode (median SEE = 3.3 kbar, mean SEE = 3.20 kbar, and mode SEE = 4.0 kbar). R^2 shows the best performance for the mean ($R^2 = 0.863$) and median ($R^2 = 0.861$) both of which offer significant improvements compared to the model using a modal estimate for prediction ($R^2 = 0.782$).

3.3. Inclusion of Equilibrium Liquids

Major element partitioning within the crystal structure of clinopyroxene is not solely sensitive to pressure and temperature but also dependent on chemical availability of elements in the residual liquid (melt). Thus, in systems for which both clinopyroxene and equilibrium melt chemistry are available, we have also calibrated a clinopyroxene-liquid thermobarometer in addition to the clinopyroxene only model we have presented thus far. All points in the calibration data set included liquid. Performance testing of the two models (Figure 4) reveals that, as expected, the model performs more favorably when liquid data are included as this helps to isolate the pressure-temperature dependence from the melt compositional dependence in the clinopyroxene. Figure 4 shows that liquid model curves have a higher point density at 0 for the residuals, and IQR ranges closer to 0. For pressure,

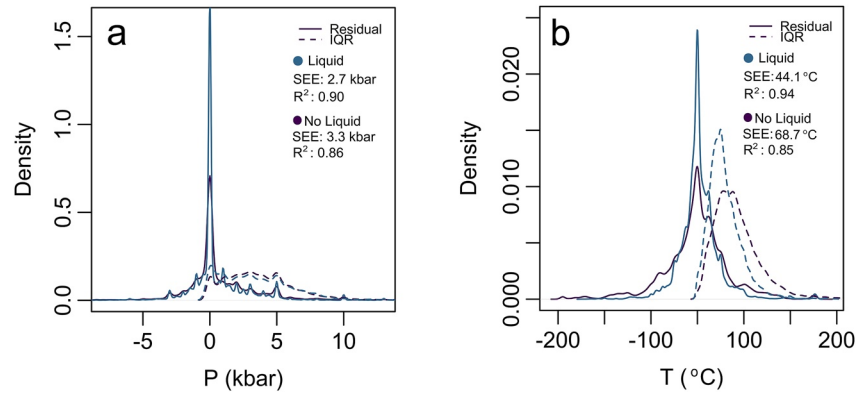

Figure 4. Residuals (solid) and IQR (dashed) density plots for liquid and no liquid models, plots are for pressure (a) and temperature (b).

the SEE decreases by 0.5 kbar and the R^2 changes from 0.86 to 0.90. For temperature, the difference is even more striking where the SEE decreases by almost half from 68.7°C to 44.1°C and the R^2 improves from 0.85 to 0.94.

4. Discussion

4.1. Mean, Mode, and Median: Which to Use?

Fundamentally, if the distribution of decision trees produces a perfect Gaussian distribution, then using the mean, which is the default of `extraTrees`, is appropriate. However, the distribution is often not a perfect Gaussian curve. Additionally, some voting distributions may have very wide uniform distributions also indicating an estimate with a low degree of certainty. Other voting distributions show sharp peaks at a given value followed by small, wide tails to low and/or high pressure/temperature. Such tails from poorly performing trees lead to overestimates of pressure or temperature due to unfair weighting by the mean of the distribution. Poorly behaving trees can result from elements being selected for decision tree nodes, which do not have a strong control on the variation of clinopyroxene unit cell parameters: these features ultimately govern the relationship between pressure, temperature, and mineral chemistry (Nimis & Ulmer, 1998).

Mean, median, and modal models all perform well although the residuals from the modal and median model are preferable to the mean (Figure 3d). Considering the R^2 of modal versus median model estimates, modal estimates (0.782) are lower than that of the median (0.861). Despite the modal model showing a marginally tighter distribution of residuals, it has a fundamental flaw that is shown in Figure 5. Here, 10% of the calibration data set was randomly extracted and a pressure gap between 5 and 15 kbar was forced into the training data set. When

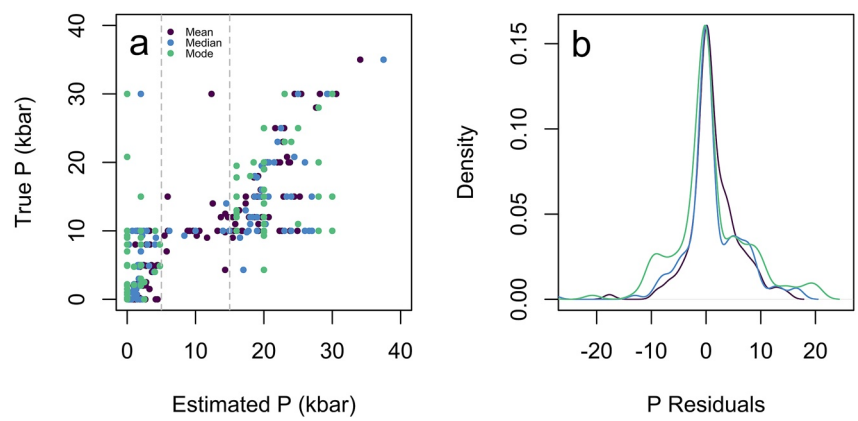

Figure 5. Results from a model with a pressure gap from 5 to 15 kbar forced into the calibration data set (gray dashed lines). Clearly seen in a and b is the poor performance of the modal estimates.

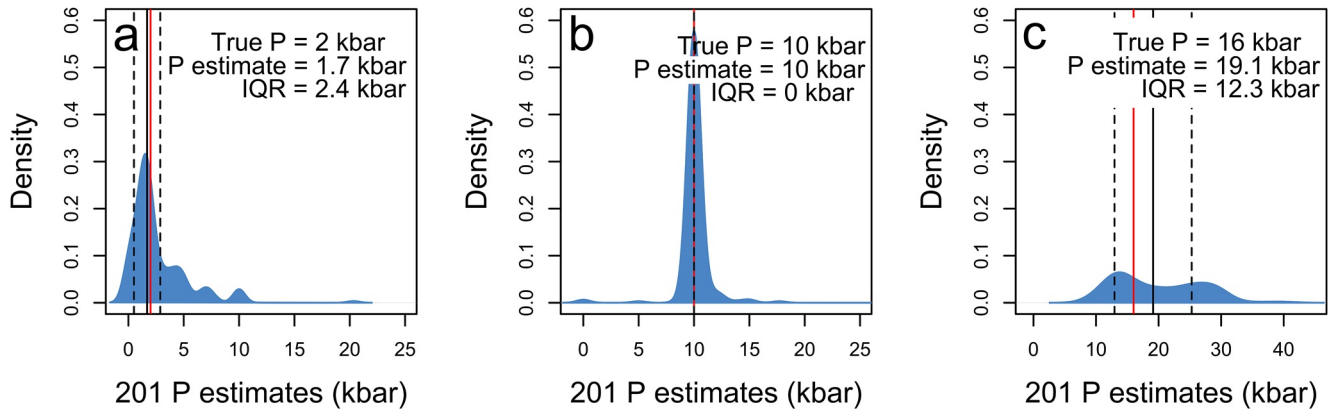

Figure 6. Figure explaining the components of the IQR and showing examples of samples which have generated an average (a), high (c), and low (b) IQR. Samples plotted here are the 201 estimates given from one forest for one sample. The solid black vertical line is the estimated pressure using the median method, the solid red vertical line is the true pressure, and the two black vertical dashed lines represent the IQR. Text on the plot shows the true pressure, estimated pressure and interquartile range, all in kbar.

the testing set is run in this pressure gapped model, the mode cannot interpolate any points in this pressure gap. Conversely, the median and mean models can close this gap by averaging values. Of course, this is an exaggerated example, but it will indeed happen on smaller scales as experiments are often lacking in intermediate values (Hirschmann et al., 2008). Natural mineral chemistry typically shows a mixture of punctuated and continuous variability (Armienti et al., 2007; Conticelli et al., 2010). Thus, we suggest that all users adopt a median value for the PT estimates.

4.2. Evaluating the Estimation Uncertainty

Throughout the course of this work, we have optimized each model to give the best representation of the true (experimental) pressure and temperature. Though we have tested and optimized each model, there remain datapoints with high residuals, giving a poor estimate relative to the true experimental value (e.g., Figure 3). With natural samples, the true pressure or temperature value is unknown and if they exist in natural data sets, these anomalous samples cannot be identified. Thus far, we have assessed the overall performance of the calibrated models by using a mean SEE for each model (Figure 2). However, this averaged SEE characterizes the model's ability to predict an entire test data set and so does not provide a unique representation of the uncertainty of any specific sample. To permit closer assessment of uncertainty, we use the interquartile range (IQR) of the voting distribution (Figure 6) to assign the confidence interval of individual natural samples. The premise is that although certain individual trees may perform poorly (see Methods above), a model that performs well overall will result in a high number of trees, predicting a pressure or temperature close to the true value. This will manifest in a voting distribution that is tight, indicating that the model has a high degree of certainty in its prediction. Users are encouraged to investigate the distributions of the PT estimates, especially in the case of a bimodal distribution or a particularly skewed distribution.

To understand why some samples yield a high IQR and some low, we can examine the test and train data sets to look at some examples of significant variations in IQR. In Figure 6, we see three examples of pressure estimates, provided by the 201 trees, represented by a density curve. The solid black vertical line is the estimated pressure using the median method, the solid red vertical line is the true pressure, and the two black vertical dashed lines represent the IQR. In Figure 6a, we see a standard IQR value, where the true (2.0 kbar) and estimated (1.7 kbar) pressures are relatively close and the IQR is a reasonable value (2.4 kbar). Figure 6b shows the ideal case where the IQR is too small to see on the plot, and the estimated and true pressures are identical (10.0 kbar). Figure 6c shows an example with a large IQR (12.3 kbar) and different true (16.0 kbar) and estimated (19.1 kbar) pressures. In this final case, we see that the true pressure is still plotting within the IQR; however, we recommend users treat any data with an IQR higher than double the overall model SEE with a healthy amount of caution. Additionally, we stress that users should consider their results within a textural context to see the effect on zoning patterns (resorption, sector zoning, and disequilibrium) with respect to the PT estimates as well as the IQR.

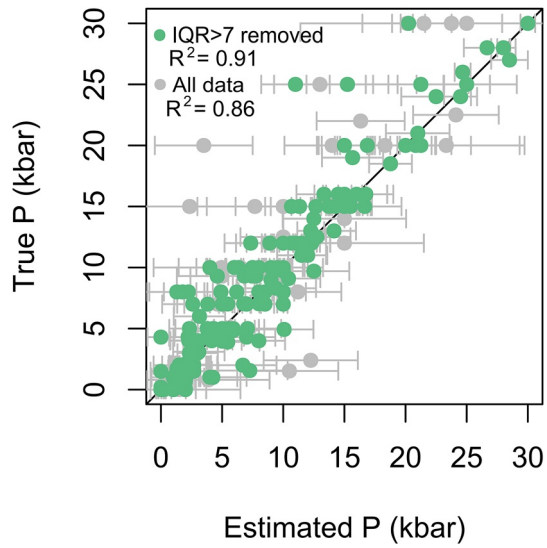

Figure 7. Single split of the test/train data set plotted with the IQR as one would with error bars in gray. Points in gray are all the data and in green represent the data filtered to remove any data with an IQR larger than 7 kbar.

The user may either present their natural data with the IQR as an uncertainty (e.g., error bar) or use the IQR as a metric for post-estimate filtering. Figure 7 shows the results of a single split of the test and train data set in gray points. This plot shows IQR plotted as pseudo error bars in which almost all points within their IQR ranges lie on the 1:1 line. The datapoints in green show an example of IQR filtering, where data with an IQR larger than 7 are removed. We observe that points qualitatively identified as outliers are removed by this filtering, and the points that remain plot close to the 1:1 line. The same principle can be applied to temperature estimates. This approach encourages users to carefully consider their own data on a point-by-point basis to determine their contribution to the final target of the study. Analyses returning a low IQR may be considered more robust, and interpretations can be based on these points with greater confidence. This is a noteworthy and novel advantage of random forest thermobarometry with respect to other methods.

4.3. Pressure Filtering

Experiments that are performed under pressurized conditions require complex machinery and sometimes large time commitments (Holloway & Wood, 2012; Kägi et al., 2005; Leinenweber et al., 2012). Thus, the suite of data in the calibration data set is heavily skewed toward experiments carried out at lower pressures (≤2 kbar). This is especially true for experiments performed at 1 atm, which comprise 29% of the filtered calibration data set, likely owing to the limited range over, which pressure assemblies can effectively and safely operate at magmatic temperatures (Shaw, 2018b). We had concerns that this might unevenly skew the barometer estimates to lower pressures. To test this, we ran several models: the base model (or "mantle model"; $P \leq 30$ kbar) and the "crustal model" ($P \leq 15$ kbar) as chosen for the crustal range on the basis of the average crustal thickness (Kopp et al., 2011; MacKenzie et al., 2008; Tewari et al., 2018). Finally, we ran these two models with 1 atm experiments included and excluded.

As seen in Figure 8, there is not a strong effect on the residuals for the four models in pressure or temperature space. There is a slight effect on the IQR with the density curves of crustal models for both pressure and temperature, showing a higher density of low IQR values than the mantle model, and the density of the pressure residuals seems to be minorly denser at 0 for the crustal model (Figure 8). Considering this quantitatively, we assess the average R^2 and SEE values over the 200 test and train data set splits. For the "mantle-1 atm" in the model, the SEE is 3.3 kbar and 68.6°C, and R^2 of 0.86 for pressure and 0.85 for temperature, whereas the "crustal-1 atm in" model gives a lower SEE of 2.4 kbar and 68.6°C and but a much lower R^2 of 0.76 for the pressure model and 0.77 for the temperature model. When we consider the 1 atm excluded models, the "mantle-1 atm out" model gives an SEE of 3.2 and 65.0°C and an R^2 of 0.85 for pressure and 0.87 for temperature, and the crustal model shows a similar trend of a lower SEE 2.3 kbar and 62.9°C and a worse R^2 of 0.75 for pressure and 0.82 for temperature.

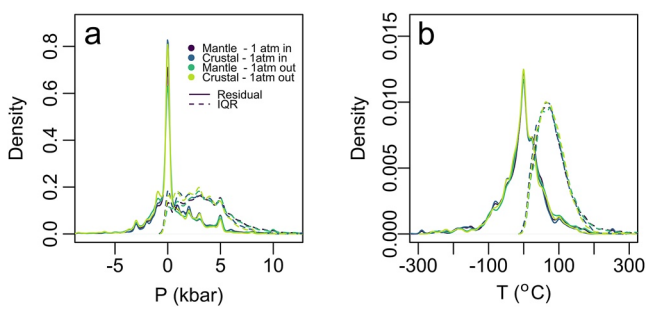

Figure 8. Residuals (solid) and IQR (dashed) density plots for the pressure filtered models mantle (0–30 kbar), crustal (0–15 kbar) with and without the 1 atm experiments. Plots are for pressure (a) and temperature (b).

Given this information, we must also consider one of the most striking limitations of a random forest algorithm—that it cannot extrapolate data. This means that natural clinopyroxenes crystallized within the mantle, which are input into a crustal model, may yield anomalously low-pressure estimates. Thus, even though the crustal model has shown slight advantages with respect to IQR and average SEE, we suggest that users employ the mantle model with the 1 atm experiments included. This is even more critical for compositions where experimental data are sparse. Alternatively, the "choose your own adventure" code contains instructions for tailoring models to user requirements, such as changing bounds of pressure filtering for application to areas with thicker (continental) crust (Bloch et al., 2017).

4.4. Adding Liquid Data to the Model

As demonstrated in Figure 4, adding equilibrium liquid data improves the model (SEE is lower by >0.5 kbar and >30°C), and so quantitatively it seems favorable to use liquid data if it is available to users. In nature, however, opportunities for reliable coexisting melt measurement may be rare. Melt inclusions have been shown to suffer from post-entrapment crystallization, which alters their composition of the melt inclusion (Bucholz et al., 2013; Danyushevsky et al., 2002; Steele-macinnis et al., 2011) or precipitation of daughter minerals at the edges of the melt inclusions (Moore & Carmichael, 1998; Venugopal et al., 2020). Additionally, melt inclusions may be absent in crystals or overrepresented in core or rim domains due to favorable growth along cracked surfaces (Faure & Schiano, 2005) or during heating, dissolution, and reprecipitation (Cashman & Blundy, 2013; Edmonds et al., 2016; Nakamura & Shimakita, 1998). Measuring matrix glass and crystal rim as the mineral-liquid pair is the most common metric for clinopyroxene—liquid thermobarometry. This may generate a bias in P-T estimates toward the final equilibration conditions of the upper part of the magmatic system. Previous works have investigated the use of melt matching algorithms to circumvent lack of liquid but others have found this to impose an additional uncertainty to the estimates so we did not explore further (Neave et al., 2019; Neave & Putirka, 2017; Petrelli et al., 2020).

By using single-phase thermobarometers, the entire protracted history of the crystal can be measured, which can recover the full extent of crystallization P-T in trans crustal magmatic systems (Annen et al., 2006; Christopher et al., 2015; Sparks et al., 2019). Regardless, the performance of the liquid model is clearly superior to the crystal only model, so we suggest that users of the clinopyroxene-liquid model keep a detailed petrological record of melt inclusions including distribution in the crystal and occurrence of mineral precipitation at melt inclusion margins.

5. Conclusions

We have shown that machine learning is a powerful and versatile approach to thermobarometry in agreement with other studies (Higgins et al., 2022; Petrelli et al., 2020). Through detailed testing, we have determined models that have an SEE comparable to the leading clinopyroxene thermobarometers (SEE of 3.2 kbar, 47.6°C and 4.4 kbar, 76.0°C for the liquid and no liquid models, respectively, as compared to 3.4 kbar and 125°C for the alkaline only liquid-cpx models of Masotta et al. (2013); 1.4 kbar for the mafic models of Neave and Putirka (2017); 3.1 kbar, 2.94 kbar, and 31.4°C from equation 32a, 32c, and 33, respectively, in (Putirka et al., 1996); 2.68 kbar and 93°C for the Wang et al. (2021) model). This thermobarometer can be applied to a wider range of compositions with a similar performance as existing models. Additionally, this model as has the added benefit of error analysis on individual estimates, where users can discard poorly performing estimates if they desire. Currently, no thermobarometer is accurate enough to resolve small distinct chambers within the upper or lower crust due to residuals exceeding 1–2 kbar. Our thermobarometer remains a powerful tool used in conjunction with textural data to constrain upper and lower crustal crystallization. Our extensive calibration data set means our models are highly suited for the global range of melt compositions. Additionally, when used in combination with the IQR of the voting distributions, users can further constrain accuracy of the pressure and temperature estimates and uniquely filter these values rather than relying merely on a single SEE assessment.

Hyperparameters generally make little difference to the performance of the thermobarometer. The largest effect is the value of `mtry`, which at low values (1 or 2) yields poor model performance (Figure 2). Instead, the largest effect on model performance is the method of output determination, that is, whether the mean, median, or mode of the voting distribution is used to recover pressure and temperature. Here, we reveal that although the mean can provide reasonable pressure and temperature estimates, natural data for which analogous experiments are sparse may yield anomalously high-pressure predictions for low-pressure experiments. The mode, on the other hand, gives values with the lowest residuals but struggles to reproduce data reliably in significant pressure and temperature gaps (Figure 5a). Thus, we recommend a semi-automated approach where users filter their data using the interquartile range of the voting distribution but rely on the median value of the predicted pressure and temperature by default. This allows for consistently lower residual values when predicting experimental data.

Two sets of codes have been created, with detailed comments and instructions, for the Earth sciences community to rapidly predict intensive parameters for natural data or create more tailored models (Appendix A). The purpose of this paper is to provide a framework for use of machine learning thermobarometry in Earth Sciences for users of widely differing computing experience. We believe that our model, given the right considerations, can result in

a high-resolution study of crustal magmatic systems. This also provides a general strategy for a machine learning approach to a single phase thermobarometry, which can be applied to other minerals. Future work will focus on testing the model with chemically independent pressure and temperature estimates and show examples of how this model can be used for different melt compositions.

Appendix A: Code Distribution and Usage

Our methodology can be widely implemented within the volcanology and petrology community. We have created two versions of the models, which we are fondly calling the "Choose your own adventure" (CYOA) model and the "Plug and play" (PnP) model. Both versions are available on Github as a comprehensive R script for download at https://github.com/corinjorgenson/RandomForest-cpx-thermobarometer and archived on Zenodo at https://zenodo.org/record/5838122#.Yd7qmv7MI2x (Jorgenson et al., 2021). In this section, we will describe how to use each of the scripts. Users who are not familiar with R are directed to "YaRrr! The Pirate's Guide to R," where Chapter 2 has instructions for installation (https://bookdown.org/ndphillips/YaRrr/installing-base-r-and-rstudio.html Phillips, (2017). Users should have at least R version 3.5 for best results. Users who prefer to use python will find in the Supporting Information S1 python functions that modify the standard implementation of the python Exrta Trees regressor.

1. Choosing the model

   The "Plug and Play" models are created using a defined set of major oxides, which a user must have in their data to use the model. The elements are SiO_2, TiO_2, Al_2O_3, Cr_2O_3, FeO, MgO, MnO, CaO, and Na_2O for the clinopyroxene analysis and SiO_2, TiO_2, Al_2O_3, FeO, MgO, MnO, CaO, Na_2O, and K_2O for the liquid analysis. If users do not have these elements, then they must use the "Choose your own adventure" and adjust what elements are used to calibrate the model. Liquid analysis should be in equilibrium with the clinopyroxene host and the two measurements should be taken where they are in apparent equilibrium. We recommend users input their data into the.csv file "InputData," while retaining the same column headers. If a user does not have liquid data, then they should leave columns blank or put zeros in place.

2. Choose your own adventure

   This folder comprises seven separate R scripts, which should be run in sequential order. The folder also includes the initial calibration data set as a.csv file, an example natural data set, and an R data file with oxide weights titled `cpx_dat`, `YOUR_DATA`, and `OxiWeight.Rdata`, respectively. A brief explanation of usage can be found in a.txt file titled README. Here, we will sequentially discuss the code for each file. We recommend between running each script, the user clears the environment and reloads the necessary files to preserve computer memory. While running this code, users should keep a keen eye on the console in case of any errors. If there are any errors, we advise clearing the environment and rerunning the code. Most of the scripts should run on the order of seconds, except for script #4. As a benchmark, running the entire CYOA cpx-liq model on a PC (i7, 4 cores, 16GB of RAM) takes 3–5 min.

   i. Preprocessing—cpx thermobaro

      This script is used for preprocessing of the calibration data set (Table S1 in Supporting Information S1). All mineral data are recalculated according to their respective structural formula following the methodology of Deer et al. (1997). This script converts any reported Fe_2O_3 to FeO and normalizes the liquid data to 100 wt% anhydrous. The output is a file called `raw.Rdata`. You do not need to change anything in this sheet unless you change the calibration data set (e.g., to add new experimental data from the scientific literature). If the user decides to add new experiments to the calibration data set, it is imperative that they format the new data in the same way that the calibration data set is currently formatted.

   ii. Filtering—cpx thermobaro

      This script is used for filtering of the calibration data set. Our choices of chemical and P-T filters can be found in Section 2.1. The user does not need to change anything in this script unless they desire alternative filtrations (i.e., specific compositional or pressure filters).

Data output from script 1 (called `raw`) should be reloaded into the environment. This file is renamed to `dat`, and an extra column called `Rm` is added to the data frame, which will have either a `Y` or `N`, which dictates if data should be filtered `(Y)` or not `(N)`.

As outlined in Section 2.1, the Kd provides a test for equilibrium between clinopyroxene and based on the Fe/Mg ratio and can be used to filter poor quality data. Additionally, samples can be removed from the calibration data set >30 kbar where data are very sparse. Lastly, we filter for extremely low liquid SiO_2 contents, which we have set as 35 wt.% SiO_2 and abnormally high clinopyroxene K_2O above 1.5 wt.%.

The data are filtered so the samples that were assigned Y to the Rm column are removed. Finally, the calibration data set is mixed to avoid bias from the organization of the data. This filtered data frame is called `input` and saved as an Rdata file.

iii. Distribute Grid Search

The scripts Distribute Grid Search and Determine SEE are used to calculate the SEE for the final models. Two hundred test and training data sets are extracted and the model is run 200 times. This yields a distribution of SEE on which the modal SEE to be assigned to the model is calculated (see Section 2.3 for details). The number of test and train splits may be changed from the default by the user if required.

In detail, the calibration data set is first loaded as `input.Rdata`. The number of test and train data sets is selected using the variable `r`. The test data set is ~10% depending on how many points are present in the calibration data set (`input`). In the for loop (which runs `r = 200` times), a grid system is defined where P/T upper/lower are the bounds for each grid square. `perms` provides all possible combinations for the lower P and *T* bounds and is summed with the upper bounds. `sam` is the grid, which is sampled in `samp`. One sample is selected from each of the grid squared and is added to `perms`. From `perms`, we determine the number of points in each of the grid squares and the grid squares with less than two points are removed from the sampled point (`no.perms`). Finally, the samples from each of the grid squares (`perms`) are called `test.ids`. The identities of the training data set are determined (those not present in `test.ids`) and assigned to the variable `train.ids`. Both the `test.ids` and `train.ids` are saved as `.Rdata` files.

iv. Determine SEE—cpx thermobaro

This code determines the average SEE for the P and T models. In this script, the user may add or remove liquid data. It is imperative that the conditions used for this script are the same as script #5. We strongly recommend you clear the environment before using this script.

The calibration data set is loaded into the environment as `input.Rdata` and the test and train ids are loaded as `testids.Rdata` and `trainids.Rdata` from the previous script. Next, users can decide if they want to include liquid data in the model `(liq <- c("Liquid"))` or not `(liq <- c("No-Liquid"))`. Next, elements used as features in the model are selected. The order of these elements must be the same in this script as in script #5 or the model will read the wrong elements and return a very poor prediction. Elements for the clinopyroxene are defined as the variable `ox` and for the liquid phase as `liqox`. Next, the `r` value (200, as in script #3) and hyperparameters are defined. We direct the reader to Section 3.1 for further information. Lastly, 1 atm experiments can be included or excluded. The calibration data set at this stage is renamed `dat` for the rest of the script.

Objects `id.test` and `id.train` are used to determine the ids of the test/train sets in the `dat` (calibration data set) data frame. A set of empty lists are made for the data to be filled into. The for loop is run `r` (defaut = 200) times. For each run, the training data set is used to create the model and the test data set is input into the model from which the pressures are estimated using the median pressure determination. From this estimated pressure, the residuals, R^2 and SEE, are calculated. This is repeated for pressure and temperature and finally loaded into output, which is reduced and saved as `final.Rdata`. From these 200 runs, the average SEE is determined by calculating the average SEE. This script has the longest computational time. During the run time, `j` is printed in the console twice (up to 200 times, once for pressure and once for temperature) to update the user on the model progress.

The mean, median, and modal pressures are calculated. As discussed in the text, we suggest that users select the median estimate. Rerunning the script several times will incur minor differences in the SEE (~0.2 kbar and ~10°C). These variations are related to the randomness in the random number generator used during model generation. This effect is negligible.

v. Final Model Training—cpx thermobaro

This script generates the final model for natural data prediction. Once calibrated and saved, this model can be used continuously in script 6 for prediction of unknown data sets without the necessity of rerunning scripts 1–5 for the calibration data set. The models are formatted as random forest objects (`P_C` and `T_C` for the pressure and temperature models, respectively) and are saved as `.Rdata` files.

vi. Filter user data—cpx thermobaro

This script is the same as script #1 and #2 with some adjustments to avoid overwriting the calibration data set or your data. Users will need to change the code `userdat <-read.delim("InputData.txt")` to reflect the title of their data or copy and paste their data into the InputData.csv file (and remove the data we have there) so that the formatting is maintained. Ensure oxides are properly suffixed (`.cpx` for clinopyroxene and `.liq` for the liquid data).

vii. Run the model—cpx thermobaro

This script is the final input for user data to retrieve pressure and temperature estimates. Inputted data should be filtered by script #6. The models are loaded in as `P_C.Rdata` and `T_C.Rdata` and outputted as `predP` and `predT`, respectively. Data are loaded in and subsetted for the elements used to make the final model. It is imperative that the element order is the same as chosen for model training or the outputs will be wrong.

The code then takes the `pred P` and `predT` and calculates the respective mean, median, mode, and IQR estimates using the apply function. After the colon of each line, the data are saved as a dataframe termed `OUTPUTDATA` This `OutputData.csv` is the final file with estimated P and T values.

3. Plug and play

This script and corresponding `.Rdata` files allow the user to use our predetermined models with a precalculated SEE for either liquid or no liquid data. These models are run with `ntree` = 201, `mtry` = 6 (12 for the liquid model), `numcuts` = 1, pressures input from 0 to 30 kbar (with 1 atm included). The SEE for the liquid model is 2.7 kbar, 44.9°C, and for the no liquid models, it is of 3.2 kbar and 72.5°C.

This model assumes that the user has already filtered their data. Users should copy and paste their data into the example excel file `InpudtData.csv` and leave the column headers so the suffixes are saved. Clinopyroxene major oxides should be the same as in the model and need to be suffixed with `.cpx` even if using a no liquid model, and liquid/melt analysis should be suffixed with `.liq`. Examples and lists of the major oxides needed are listed in the script itself.

To use the script users will need to first open R studio and comment (add a #) and uncomment (remove #) to reflect if they have liquid data or not. For example, if you are not using liquid data, then the code should appear as:

```
liq <- "NoLiquid"

#liq <- "Liquid"
```

If liquid data is included the code should appear as:

```
#liq <- "NoLiquid"

liq <- "Liquid"
```

After this step, the user should be able to select all the code (cmd+a for mac; ctrl+a for windows) and press run. Data are saved as a csv called `OutputData.csv`. The end of the script features some basic plots although we encourage users to delve into the wonderful world of plotting in R.

Data Availability Statement

Version 1.1 of the software Random Forest cpx-thermobarometer is preserved at https://doi.org/10.5281/zenodo.5838122, https://zenodo.org/record/5838122#.Yd7qmv7MI2x and is available via creative commons attribution. Any minor updates to the code will be available at https://github.com/corinjorgenson/RandomForest-cpx-thermobarometer.

Acknowledgments
We would like to thank all the experimental petrologist whose hours of work make this model possible. Much of their data are available at http://lepr.ofm-research.org/YUI/access_user/login.php. Thank you to Chao Zhang, Euan Mutch, and the paper editor Stephen Parman for their constructive feedback. CJ and LC received funding from the Swiss National Science Foundation (Grant No. 200021_184632). OH and LC received funding from the European Research Council (ERC) under the European Union's Horizon 2020 research and innovation program (Grant agreement 677493 - FEVER). MP received funding from the Università degli Studi di Perugia "ENGAGE" FRB-2019 grant. Open access funding provided by Universite de Geneve.

References

Annen, C., Blundy, J. D., & Sparks, R. S. J. (2006). The Genesis of intermediate and silicic magmas in deep crustal hot zones. *Journal of Petrology*, *47*(3), 505–539. https://doi.org/10.1093/petrology/egi084

Armienti, P., Tonarini, S., Innocenti, F., & D'Orazio, M. (2007). Mount Etna pyroxene as tracer of petrogenetic processes and dynamics of the feeding system. *Special Papers - Geological Society of America*, *418*(January 2007), 265–276. https://doi.org/10.1130/2007.2418(13)

Behrens, H., Misiti, V., Freda, C., Vetere, F., Botcharnikov, R. E., & Scarlato, P. (2009). Solubility of H_2O and CO_2 in ultrapotassic melts at 1200 and 1250°C and pressure from 50 to 500 MPa. *American Mineralogist*, *94*(1), 105–120. https://doi.org/10.2138/am.2009.2796

Bloch, E., Ibañez-Mejia, M., Murray, K., Vervoort, J., & Müntener, O. (2017). Recent crustal foundering in the Northern Volcanic Zone of the Andean arc: Petrological insights from the roots of a modern subduction zone. *Earth and Planetary Science Letters*, *476*, 47–58. https://doi.org/10.1016/j.epsl.2017.07.041

Breiman, L. (2001). Random forests. *Machine Learning*, *45*, 5–32. https://doi.org/10.1023/a:1010933404324

Breiman, L. (2002). Manual on setting up, using, and understanding random foest V3.1. *Statistics Department University of California*. *1*(58).

Bucholz, C. E., Gaetani, G. A., Behn, M. D., & Shimizu, N. (2013). Post-entrapment modification of volatiles and oxygen fugacity in olivine-hosted melt inclusions. *Earth and Planetary Science Letters*, *374*, 145–155. https://doi.org/10.1016/j.epsl.2013.05.033

Cashman, K., & Blundy, J. (2013). Petrological cannibalism: The chemical and textural consequences of incremental magma body growth. *Contributions to Mineralogy and Petrology*, *166*(3), 703–729. https://doi.org/10.1007/s00410-013-0895-0

Christopher, T., Blundy, J., Cashman, K., Cole, P., Edmonds, M., Smith, P., et al. (2015). Geochemistry, geophysics, geosystems. *Geochemistry, Geophysics, Geosystems*, *18*(1–2), 1541–1576. https://doi.org/10.1002/2015GC005791

Conticelli, S., Boari, E., & Avanzinelli, R. (2010). *The colli albani volcano*. Speical Publications of IAVCEI. Issue.3.

Danyushevsky, L. V., McNeill, A. W., & Sobolev, A. V. (2002). Experimental and petrological studies of melt inclusions in phenocrysts from mantle-derived magmas: An overview of techniques, advantages and complications. *Chemical Geology*, *183*(1–4), 5–24. https://doi.org/10.1016/S0009-2541(01)00369-2

Deer, W. A., Howie, R. A., & Zussman, J. (1997). *Rock-forming minerals: Single-chain silicates* (Vol. 2A). Geological Society of London.

Edmonds, M., Kohn, S. C., Hauri, E. H., Humphreys, M. C. S., & Cassidy, M. (2016). Extensive, water-rich magma reservoir beneath southern Montserrat. *Lithos*, *252–253*, 216–233. https://doi.org/10.1016/j.lithos.2016.02.026

Faure, F., & Schiano, P. (2005). Experimental investigation of equilibration conditions during forsterite growth and melt inclusion formation. *Earth and Planetary Science Letters*, *236*(3–4), 882–898. https://doi.org/10.1016/j.epsl.2005.04.050

Georgeais, G., Koga, K. T., Moussallam, Y., & Rose-Koga, E. F. (2021). Magma decompression rate calculations with EMBER: A user-friendly software to model diffusion of H_2O, CO_2 and S in melt embayments. *Geochemistry, Geophysics, Geosystems*, *22*. https://doi.org/10.1029/2020gc009542

Ghiorso, M. S., & Gualda, G. A. R. (2015). An H_2O–CO_2 mixed fluid saturation model compatible with rhyolite-MELTS. *Contributions to Mineralogy and Petrology*, *169*(6), 1–30. https://doi.org/10.1007/s00410-015-1141-8

Ghiorso, M. S., & Wolf, A. S. (2019). Thermodynamic modeling using ENKI: 1. *Overview and Phase Equilibrium Applications*.

Giacomoni, P. P., Coltorti, M., Bryce, J. G., Fahnestock, M. F., & Guitreau, M. (2016). Mt. Etna plumbing system revealed by combined textural, compositional, and thermobarometric studies in clinopyroxenes. *Contributions to Mineralogy and Petrology*, *171*(4), 1–15. https://doi.org/10.1007/s00410-016-1247-7

Higgins, O., Sheldrake, T., & Caricchi, L. (2022). Machine learning thermobarometry and chemometry using amphibole and clinopyroxene: A window into the roots of an arc volcano (Mount Liamuiga, Saint Kitts). *Contributions to Mineralogy and Petrology*, *177*, 10. https://doi.org/10.1007/s00410-021-01874-6

Hirschmann, M. M., Ghiorso, M. S., Davis, F. A., Gordon, S. M., Mukherjee, S., Grove, T. L., et al. (2008). Library of experimental phase relations (LEPR): A database and web portal for experimental magmatic phase equilibria data. *Geochemistry, Geophysics, Geosystems*, *9*(3), a–n. https://doi.org/10.1029/2007GC001894

Ho, T. K. (1995). Random decision forests. *Proceedings of the International Conference on Document Analysis and Recognition, ICDAR*, *1*, 278–282. https://doi.org/10.1109/ICDAR.1995.598994

Holloway, J. R., & Wood, B. J. (2012). *Simulating the Earth: Experimental geochemisty*. Springer Science & Business.

Iacovino, K., Matthews, S., Wieser, P. E., Moore, G. M., & Bégué, F. (2020). VESIcal Part I: An open-source thermodynamic model engine for mixed volatile (H_2O-CO_2) solubility in silicate melts. *Preprint: Earth and Space Science*, 1–58.

Jorgenson, C., Higgins, O., Petrelli, M., Bégué, F., & Caricchi, L. (2021). corinjorgenson/RandomForest-cpx-thermobarometer: RandomForest-cpx-thermobarometer code (v2.0). *Zenodo*. https://doi.org/10.5281/zenodo.5838122

Kägi, R., Müntener, O., Ulmer, P., & Ottolini, L. (2005). Piston-cylinder experiments on H_2O undersaturated Fe-bearing systems: An experimental setup approaching fO_2 conditions of natural calc-alkaline magmas. *American Mineralogist*, *90*(4), 708–717. https://doi.org/10.2138/am.2005.1663

Klügel, A., & Klein, F. (2006). Complex magma storage and ascent at embryonic submarine volcanoes from the Madeira Archipelago. *Geology*, *34*(5), 337. https://doi.org/10.1130/G22077.1

Kopp, H., Weinzierl, W., Becel, A., Charvis, P., Evain, M., Flueh, E. R., et al. (2011). Deep structure of the central lesser antilles island arc: Relevance for the formation of continental crust. *Earth and Planetary Science Letters*, *304*(1–2), 121–134. https://doi.org/10.1016/j.epsl.2011.01.024

Leinenweber, K. D., Tyburczy, J. A., Sharp, T. G., Soignard, E., Diedrich, T., Petuskey, W. B., et al. (2012). Cell assemblies for reproducible multi-anvil experiments (the COMPRES assemblies). *American Mineralogist*, *97*(2–3), 353–368. https://doi.org/10.2138/am.2012.3844

Lemenkova, P. (2019). An empirical study of R applications for data analysis in marine geology. *Marine Science and Technology Bulletin*, *8*, 1–9. https://doi.org/10.33714/masteb.486678

Lubbers, J., Kent, A. J. R., Meisenheimer, D. E., & Wildenschild, D. (2019). *Using MicroCT to quantify 3D zoning in sanidine: Implications for magma reservoir processes*.

MacKenzie, L., Abers, G. A., Fischer, K. M., Syracuse, E. M., Protti, J. M., Gonzalez, V., & Strauch, W. (2008). Crustal structure along the southern Central American volcanic front. *Geochemistry, Geophysics, Geosystems*, *9*(8). https://doi.org/10.1029/2008GC001991

Masotta, M., Mollo, S., Freda, C., Gaeta, M., & Moore, G. (2013). Clinopyroxene–liquid thermometers and barometers specific to alkaline differentiated magmas. *Contributions to Mineralogy and Petrology*, *166*(6), 1545–1561. https://doi.org/10.1007/s00410-013-0927-9

Moore, L. R., Mironov, N., Portnyagin, M., Gazel, E., & Bodnar, R. J. (2018). Volatile contents of primitive bubble-bearing melt inclusions from Klyuchevskoy volcano, Kamchatka: Comparison of volatile contents determined by mass-balance versus experimental homogenization. *Journal of Volcanology and Geothermal Research*, *358*, 124–131. https://doi.org/10.1016/j.jvolgeores.2018.03.007

Nakamura, M., & Shimakita, S. (1998). Dissolution origin and syn-entrapment compositional change of melt inclusion in plagioclase. *Earth and Planetary Science Letters*, *161*(1–4), 119–133. https://doi.org/10.1016/S0012-821X(98)00144-7

Neave, D. A., Bali, E., Guðfinnsson, G. H., Halldórsson, S. A., Kahl, M., Schmidt, A. S., & Holtz, F. (2019). Clinopyroxene-liquid equilibria and geothermobarometry in natural and experimental tholeiites: The 2014-2015 holuhraun eruption, Iceland. *Journal of Petrology*, *60*(8), 1653–1680. https://doi.org/10.1093/petrology/egz042

Neave, D. A., & Putirka, K. D. (2017). A new clinopyroxene-liquid barometer, and implications for magma storage pressures under Icelandic rift zones. *American Mineralogist*, *102*(4), 777–794. https://doi.org/10.2138/am-2017-5968

Newman, S., & Lowenstern, J. B. (2002). Volatilecalc: A silicate melt-H_2O-CO_2 solution model written in visual basic for excel. *Computers & Geosciences*, *28*(5), 597–604. https://doi.org/10.1016/S0098-3004(01)00081-4

Nimis, P., & Taylor, W. R. (2000). Single clinopyroxene thermobarometry for garnet peridotites. Part I. Calibration and testing of a Cr-in-Cpx barometer and an enstatite-in-Cpx thermometer. *Contributions to Mineralogy and Petrology*, *139*(5), 541–554. https://doi.org/10.1007/s004100000156

Nimis, P., & Ulmer, P. (1998). Clinopyroxene geobarometry of magmatic rocks. Part 1: An expanded structural geobarometer for anhydrous and hydrous, basic and ultrabasic systems. *Contributions to Mineralogy and Petrology*, *133*(1–2), 122–135. https://doi.org/10.1007/s004100050442

Oshiro, T. M., Perez, P. S., & Baranauskas, J. A. (2012). How many trees in a random forest? In *Lecture notes in computer science (including subseries lecture notes in artificial intelligence and lecture notes in bioinformatics)* (pp. 154–168). 7376 LNAI. https://doi.org/10.1007/978-3-642-31537-4_13

Petrelli, M., Caricchi, L., & Perugini, D. (2020). Machine learning thermo - barometry: Application to clinopyroxene - bearing magmas journal of geophysical research : Solid Earth. *Journal of Geophysical Research: Solid Earth*, *125*. https://doi.org/10.1029/2020JB020130

Phillips, N. D. (2017). YaRrr! The Pirate's Guide to R.

Probst, P., & Boulesteix, A. L. (2018). To tune or not to tune the number of trees in random forest. *Journal of Machine Learning Research*, *18*, 1–8.

Probst, P., Wright, M. N., & Boulesteix, A. L. (2019). Hyperparameters and tuning strategies for random forest. *Wiley Interdisciplinary Reviews: Data Mining and Knowledge Discovery*, *9*(3), 1–15. https://doi.org/10.1002/widm.1301

Putirka, K. (1999). Clinopyroxene + liquid equilibria to 100 kbar and 2450 K. *Contributions to Mineralogy and Petrology*, *135*(2–3), 151–163. https://doi.org/10.1007/s004100050503

Putirka, K. (2016). Amphibole thermometers and barometers for igneous systems and some implications for eruption mechanisms of felsic magmas at arc volcanoes. *American Mineralogist*, *101*(4), 841–858. https://doi.org/10.2138/am-2016-5506

Putirka, K. D. (2008). Thermometers and barometers for volcanic systems. *Reviews in Mineralogy and Geochemistry*, *69*, 61–120. https://doi.org/10.2138/rmg.2008.69.3

Ridolfi, F., Puerini, M., Renzulli, A., Menna, M., & Toulkeridis, L. (2008). The magmatic feeding system of El Reventador volcano (Sub-Andean zone, Ecuador) constrained by texture, mineralogy and thermobarometry of the 2002 erupted products. *Journal of Volcanology and Geothermal Research*, *176*, 94–106. https://doi.org/10.1016/j.jvolgeores.2008.03.003

Ridolfi, F., & Renzulli, A. (2012). Calcic amphiboles in calc-alkaline and alkaline magmas: Thermobarometric and chemometric empirical equations valid up to 1,130°C and 2.2 GPa. *Contributions to Mineralogy and Petrology*, *163*(5), 877–895. https://doi.org/10.1007/s00410-011-0704-6

Ridolfi, F., Renzulli, A., & Puerini, M. (2010). Stability and chemical equilibrium of amphibole in calc-alkaline magmas: An overview, new thermobarometric formulations and application to subduction-related volcanoes. *Contributions to Mineralogy and Petrology*, *160*(1), 45–66. https://doi.org/10.1007/s00410-009-0465-7

Sage, A. J., Genschel, U., & Nettleton, D. (2020). Tree aggregation for random forest class probability estimation. *Statistical Analysis and Data Mining: The ASA Data Science Journal*, *13*(2), 134–150. https://doi.org/10.1002/sam.11446

Shane, P., & Smith, V. C. (2013). Lithos Using amphibole crystals to reconstruct magma storage temperatures and pressures for the post-caldera collapse volcanism at Okataina volcano Haroharo Haroharo caldera Rotoiti collapse Tarawera. *Lithos*, *156–159*, 159–170. https://doi.org/10.1016/j.lithos.2012.11.008

Shaw, C. S. J. (2018a). Evidence for the presence of carbonate melt during the formation of cumulates in the Colli Albani Volcanic District, Italy. *Lithos*, *310–311*, 105–119. https://doi.org/10.1016/j.lithos.2018.04.007

Shaw, C. S. J. (2018b). Igneous rock associations 22. Experimental petrology: Methods, examples, and applications. *Geoscience Canada*, *45*(2), 67–84. https://doi.org/10.12789/geocanj.2018.45.134

Simm, J., Magrans De Abril, I., & Sugiyama, M. (2014). Tree-based ensemble multi-task learning method for classification and regression. *IEICE–Transactions on Info and Systems*, *E97-D*(6), 1677–1681. https://doi.org/10.1587/transinf.E97.D.1677

Smith, D. (2013). Olivine thermometry and source constraints for mantle fragments in the Navajo Volcanic Field, Colorado Plateau, southwest United States: Implications for the mantle wedge. *Geochemistry, Geophysics, Geosystems*, *14*(3), 693–711. https://doi.org/10.1002/ggge.20065

Sparks, R. S. J., Annen, C., Blundy, J. D., Cashman, K. V., Rust, A. C., & Jackson, M. D. (2019). Formation and dynamics of magma reservoirs. *Philosophical Transactions of the Royal Society A: Mathematical, Physical & Engineering Sciences*, *377*(2139). https://doi.org/10.1098/rsta.2018.0019

Steele-macinnis, M., Esposito, R., & Bodnar, R. J. (2011). Thermodynamic model for the effect of post-entrapment crystallization on the H_2O-CO_2 systematics of vapor-saturated, silicate melt inclusions. *Journal of Petrology*, *52*(12), 2461–2482. https://doi.org/10.1093/petrology/egr052

Tewari, H. C., Rajendra Prasad, B., & Kumar, P. (2018). Global and Indian scenario of crustal thickness. In *Structure and tectonics of the Indian continental crust and its adjoining region* (2nd ed., pp. 211–224). Elsevier Inc. https://doi.org/10.1016/b978-0-12-813685-0.00009-1

Venugopal, S., Schiavi, F., Moune, S., Bolfan-Casanova, N., Druitt, T., & Williams-Jones, G. (2020). Melt inclusion vapour bubbles: The hidden reservoir for major and volatile elements. *Scientific Reports*, *10*(1), 1–14. https://doi.org/10.1038/s41598-020-65226-3

Wang, X., Hou, T., Wang, M., Zhang, C., Zhang, Z., Pan, R., et al. (2021). A new clinopyroxene thermobarometer for mafic to intermediate magmatic systems. *European Journal of Mineralogy*, *33*(5), 621–637. https://doi.org/10.5194/ejm-33-621-2021

Ziberna, L., Nimis, P., Kuzmin, D., & Malkovets, V. G. (2016). Error sources in single-clinopyroxene thermobarometry and a mantle geotherm for the Novinka kimberlite, Yakutia. *American Mineralogist*, *101*(10), 2222–2232. https://doi.org/10.2138/am-2016-5540

References From the Supporting Information

Adam, J., Oberti, R., Cámara, F., & Green, T. H. (2007). An electron microprobe, LAM-ICP-MS and single-crystal X-ray structure refinement study of the effects of pressure, melt-H_2O concentration and f O_2 on experimentally produced basaltic amphiboles. *European Journal of Mineralogy*, *19*(5), 641–655.

Almeev, R. R., Holtz, F., Ariskin, A. A., & Kimura, J. I. (2013). Storage conditions of bezymianny volcano parental magmas: Results of phase equilibria experiments at 100 and 700áMPa. *Contributions to Mineralogy and Petrology*, *166*(5), 1389–1414.

Almeev, R. R., Holtz, F., Koepke, J., Parat, F., & Botcharnikov, R. E. (2007). The effect of H_2O on olivine crystallization in MORB: Experimental calibration at 200 MPa. *American Mineralogist*, *92*(4), 670–674.

Alonso-Perez, R., Müntener, O., & Ulmer, P. (2009). Igneous garnet and amphibole fractionation in the roots of island arcs: Experimental constraints on andesitic liquids. *Contributions to Mineralogy and Petrology*, *157*(4), 541–558.

Andújar, J., Costa, F., & Martí, J. (2010). Magma storage conditions of the last eruption of Teide volcano (Canary Islands, Spain). *Bulletin of Volcanology*, *72*(4), 381–395.

Andújar, J., Costa, F., Martí, J., Wolff, J. A., & Carroll, M. R. (2008). Experimental constraints on pre-eruptive conditions of phonolitic magma from the caldera-forming El Abrigo eruption, Tenerife (Canary Islands). *Chemical Geology*, *257*(3–4), 173–191.

Andújar, J., & Scaillet, B. (2012). Experimental constraints on parameters controlling the difference in the eruptive dynamics of phonolitic magmas: The case of tenerife (canary islands). *Journal of Petrology*, *53*(9), 1777–1806.

Andújar, J., Scaillet, B., Pichavant, M., & Druitt, T. H. (2015). Differentiation conditions of a basaltic magma from Santorini, and its bearing on the production of andesite in arc settings. *Journal of Petrology*, *56*(4), 765–794.

Baker, D. R., & Eggler, D. H. (1987). Compositions of anhydrous and hydrous melts coexisting with plagioclase, augite, and olivine or low-Ca pyroxene from 1 atm to 8 kbar; application to the Aleutian volcanic center of Atka. *American Mineralogist*, *72*(1–2), 12–28.

Baker, M. B., Grove, T. L., & Price, R. (1994). Primitive basalts and andesites from the Mt. Shasta region, N. California: Products of varying melt fraction and water content. *Contributions to Mineralogy and Petrology*, *118*(2), 111–129.

Baker, M. B., & Stolper, E. M. (1994). Determining the composition of high-pressure mantle melts using diamond aggregates. *Geochimica et Cosmochimica Acta*, *58*(13), 2811–2827.

Barclay, J., & Carmichael, I. S. E. (2004). A hornblende basalt from Western Mexico: Water-saturated phase relations constrain a pressure–temperature window of eruptibility. *Journal of Petrology*, *45*(3), 485–506.

Bartels, K. S., Kinzler, R. J., & Grove, T. L. (1991). High pressure phase relations of primitive high-alumina basalts from Medicine Lake volcano, northern California. *Contributions to Mineralogy and Petrology*, *108*(3), 253–270.

Beard, C. D., van Hinsberg, V. J., Stix, J., & Wilke, M. (2019). Clinopyroxene/melt trace element partitioning in sodic alkaline magmas. *Journal of Petrology*, *60*(9), 1797–1823.

Beard, C. D., van Hinsberg, V. J., Stix, J., & Wilke, M. (2020). The effect of fluorine on clinopyroxene/melt trace-element partitioning. *Contributions to Mineralogy and Petrology*, *175*(5), 1–19.

Bender, J. F., Hodges, F. N., & Bence, A. E. (1978). Petrogenesis of basalts from the project FAMOUS area: Experimental study from 0 to 15 kbars. *Earth and Planetary Science Letters*, *41*(3), 277–302.

Berndt, J., Holtz, F., & Koepke, J. (2001). Experimental constraints on storage conditions in the chemically zoned phonolitic magma chamber of the Laacher See volcano. *Contributions to Mineralogy and Petrology*, *140*(4), 469–486.

Berndt, J., Koepke, J., & Holtz, F. (2005). An experimental investigation of the influence of water and oxygen fugacity on differentiation of MORB at 200 MPa. *Journal of Petrology*, *46*(1), 135–167.

Blatter, D. L., & Carmichael, I. S. (2001). Hydrous phase equilibria of a Mexican high-silica andesite: A candidate for a mantle origin? *Geochimica et Cosmochimica Acta*, *65*(21), 4043–4065.

Blundy, J. D., Robinson, J. A. C., & Wood, B. J. (1998). Heavy REE are compatible in clinopyroxene on the spinel lherzolite solidus. *Earth and Planetary Science Letters*, *160*(3–4), 493–504.

Bonechi, B., Perinelli, C., & Gaeta, M. (2020). Clinopyroxene growth rates at high pressure: Constraints on magma recharge of the deep reservoir of the campi flegrei volcanic district (south Italy). *Bulletin of Volcanology*, *82*(1), 1–19.

Bonechi, B., Perinelli, C., Gaeta, M., Tecchiato, V., & Fabbrizio, A. (2020). Amphibole growth from a primitive alkaline basalt at 0.8 GPa: Time-dependent compositional evolution, growth rate and competition with clinopyroxene. *Lithos*, *354*, 105272.

Botcharnikov, R. E., Almeev, R. R., Koepke, J., & Holtz, F. (2008). Phase relations and liquid lines of descent in hydrous ferrobasalt—Implications for the Skaergaard intrusion and Columbia River flood basalts. *Journal of Petrology*, *49*(9), 1687–1727.

Bulatov, V. K., Girnis, A. V., & Brey, G. P. (2002). Experimental melting of a modally heterogeneous mantle. *Mineralogy and Petrology*, *75*(3), 131–152.

Carroll, M. R., & Wyllie, P. J. (1989). Experimental phase relations in the system tonalite-peridotite-H_2O at 15 kb; implications for assimilation and differentiation processes near the crust-mantle boundary. *Journal of Petrology*, *30*(6), 1351–1382.

Chen, H. K., Delano, J. W., & Lindsley, D. H. (1982). Chemistry and phase relations of VLT volcanic glasses from Apollo 14 and Apollo 17. *Journal of Geophysical Research*, *87*(S01), A171–A181.

Conte, A. M., Dolfi, D., Gaeta, M., Misiti, V., Mollo, S., & Perinelli, C. (2009). Experimental constraints on evolution of leucite-basanite magma at 1 and 10– 4 GPa: Implications for parental compositions of roman high-potassium magmas. *European Journal of Mineralogy*, *21*(4), 763–782.

Dann, J. C., Holzheid, A. H., Grove, T. L., & McSween, H. Y., Jr. (2001). Phase equilibria of the Shergotty meteorite: Constraints on pre-eruptive water contents of Martian magmas and fractional crystallization under hydrous conditions. *Meteoritics & Planetary Sciences*, *36*(6), 793–806.

Delano, J. W. (1977). Experimental melting relations of 63545, 76015, and 76055. *Lunar and Planetary Science Conference Proceedings*, *8*, 2097–2123.

Di Carlo, I. D. A., Pichavant, M., Rotolo, S. G., & Scaillet, B. (2006). Experimental crystallization of a high-K arc basalt: The golden pumice, stromboli volcano (Italy). *Journal of Petrology*, *47*(7), 1317–1343.

Draper, D. S., Andrew duFrane, S., Shearer, C. K., Jr., Dwarzski, R. E., & Agee, C. B. (2006). High-pressure phase equilibria and element partitioning experiments on Apollo 15 green C picritic glass: Implications for the role of garnet in the deep lunar interior. *Geochimica et Cosmochimica Acta*, *70*(9), 2400–2416.

Draper, D. S., & Green, T. H. (1999). P–T phase relations of silicic, alkaline, aluminous liquids: New results and applications to mantle melting and metasomatism. *Earth and Planetary Science Letters*, *170*(3), 255–268.
Draper, D. S., & Johnston, A. D. (1992). Anhydrous PT phase relations of an aleutian high-MgO basalt: An investigation of the role of olivine-liquid reaction in the generation of arc high-alumina basalts. *Contributions to Mineralogy and Petrology*, *112*(4), 501–519.
Dunn, T., & Sen, C. (1994). Mineral/matrix partition coefficients for orthopyroxene, plagioclase, and olivine in basaltic to andesitic systems: A combined analytical and experimental study. *Geochimica et Cosmochimica Acta*, *58*(2), 717–733.
Dygert, N., Liang, Y., Sun, C., & Hess, P. (2014). An experimental study of trace element partitioning between augite and Fe-rich basalts. *Geochimica et Cosmochimica Acta*, *132*, 170–186.
Elkins, L. T., Fernandes, V. A., Delano, J. W., & Grove, T. L. (2000). Origin of lunar ultramafic green glasses: Constraints from phase equilibrium studies. *Geochimica et Cosmochimica Acta*, *64*(13), 2339–2350.
Elkins-Tanton, L. T., & Grove, T. L. (2003). Evidence for deep melting of hydrous metasomatized mantle: Pliocene high-potassium magmas from the Sierra Nevadas. *Journal of Geophysical Research*, *108*(B7).
Elkins-Tanton, L. T., Chatterjee, N., & Grove, T. L. (2003). Experimental and petrological constraints on lunar differentiation from the Apollo 15 green picritic glasses. *Meteoritics & Planetary Sciences*, *38*(4), 515–527.
Elkins-Tanton, L. T., Draper, D. S., Agee, C. B., Jewell, J., Thorpe, A., & Hess, P. C. (2007). The last lavas erupted during the main phase of the siberian flood volcanic province: Results from experimental petrology. *Contributions to Mineralogy and Petrology*, *153*(2), 191–209.
Ernst, W. G., & Liu, J. (1998). Experimental phase-equilibrium study of Al-and Ti-contents of calcic amphibole in MORB—a semiquantitative thermobarometer. *American Mineralogist*, *83*(9–10), 952–969.
Fabbrizio, A., & Carroll, M. R. (2008). Experimental constraints on the differentiation process and pre-eruptive conditions in the magmatic system of Phlegraean Fields (Naples, Italy). *Journal of Volcanology and Geothermal Research*, *171*(1–2), 88–102.
Falloon, T. J., & Danyushevsky, L. V. (2000). Melting of refractory mantle at 1·5, 2 and 2·5 GPa under anhydrous and H_2O-undersaturated conditions: Implications for the petrogenesis of high-Ca boninites and the influence of subduction components on mantle melting. *Journal of Petrology*, *41*(2), 257–283.
Falloon, T. J., Danyushevsky, L. V., & Green, D. H. (2001). Peridotite melting at 1 GPa: Reversal experiments on partial melt compositions produced by peridotite–basalt sandwich experiments. *Journal of Petrology*, *42*(12), 2363–2390.
Falloon, T. J., Green, D. H., Danyushevsky, L. V., & Faul, U. H. (1999). Peridotite melting at 1.0 and 1.5 GPa: An experimental evaluation of techniques using diamond aggregates and mineral mixes for determination of near-solidus melts. *Journal of Petrology*, *40*(9), 1343–1375.
Falloon, T. J., Green, D. H., Danyushevsky, L. V., & McNeill, A. W. (2008). The composition of near-solidus partial melts of fertile peridotite at 1 and 1·5 GPa: Implications for the petrogenesis of MORB. *Journal of Petrology*, *49*(4), 591–613.
Falloon, T. J., Green, D. H., O'Neill, H. S. C., & Hibberson, W. O. (1997). Experimental tests of low degree peridotite partial melt compositions: Implications for the nature of anhydrous near-solidus peridotite melts at 1 GPa. *Earth and Planetary Science Letters*, *152*(1–4), 149–162.
Fedele, L., Zanetti, A., Morra, V., Lustrino, M., Melluso, L., & Vannucci, R. (2009). Clinopyroxene/liquid trace element partitioning in natural trachyte–trachyphonolite systems: Insights from campi flegrei (southern Italy). *Contributions to Mineralogy and Petrology*, *158*(3), 337–356.
Feig, S. T., Koepke, J., & Snow, J. E. (2006). Effect of water on tholeiitic basalt phase equilibria: An experimental study under oxidizing conditions. *Contributions to Mineralogy and Petrology*, *152*(5), 611–638.
Feig, S. T., Koepke, J., & Snow, J. E. (2010). Effect of oxygen fugacity and water on phase equilibria of a hydrous tholeiitic basalt. *Contributions to Mineralogy and Petrology*, *160*(4), 551–568.
Forsythe, L. M., Nielsen, R. L., & Fisk, M. R. (1994). High-field-strength element partitioning between pyroxene and basaltic to dacitic magmas. *Chemical Geology*, *117*(1–4), 107–125.
Fram, M. S., & Longhi, J. (1992). Phase equilibria of dikes associated with Proterozoic anorthosite complexes. *American Mineralogist*, *77*(5–6), 605–616.
Freda, C., Gaeta, M., Misiti, V., Mollo, S., Dolfi, D., & Scarlato, P. (2008). Magma–carbonate interaction: An experimental study on ultrapotassic rocks from alban hills (central Italy). *Lithos*, *101*(3–4), 397–415.
Freda, C., Gaeta, M., Palladino, D. M., & Trigila, R. (1997). The villa senni eruption (alban hills, central Italy): The role of H_2O and CO_2 on the magma chamber evolution and on the eruptive scenario. *Journal of Volcanology and Geothermal Research*, *78*(1–2), 103–120.
Freise, M., Holtz, F., Nowak, M., Scoates, J. S., & Strauss, H. (2009). Differentiation and crystallization conditions of basalts from the kerguelen large igneous province: An experimental study. *Contributions to Mineralogy and Petrology*, *158*(4), 505–527.
Fujii, T., & Bougault, H. (1983). Melting relations of a magnesian abyssal tholeiite and the origin of MORBs. *Earth and Planetary Science Letters*, *62*(2), 283–295.
Gaetani, G. A. (2004). The influence of melt structure on trace element partitioning near the peridotite solidus. *Contributions to Mineralogy and Petrology*, *147*(5), 511–527.
Grove, T. L., Elkins-Tanton, L. T., Parman, S. W., Chatterjee, N., Müntener, O., & Gaetani, G. A. (2003). Fractional crystallization and mantle-melting controls on calc-alkaline differentiation trends. *Contributions to Mineralogy and Petrology*, *145*(5), 515–533.
Gaetani, G. A., Kent, A. J., Grove, T. L., Hutcheon, I. D., & Stolper, E. M. (2003). Mineral/melt partitioning of trace elements during hydrous peridotite partial melting. *Contributions to Mineralogy and Petrology*, *145*(4), 391–405.
Gee, L. L., & Sack, R. O. (1988). Experimental petrology of melilite nephelinites. *Journal of Petrology*, *29*(6), 1233–1255.
Giehl, C., Marks, M., & Nowak, M. (2013). Phase relations and liquid lines of descent of an iron-rich peralkaline phonolitic melt: An experimental study. *Contributions to Mineralogy and Petrology*, *165*(2), 283–304.
Girnis, A. V., Bulatov, V. K., Lahaye, Y., & Brey, G. P. (2006). Partitioning of trace elements between carbonate-silicate melts and mantle minerals: Experiment and petrological consequences. *Petrology*, *14*(5), 492–514.
Green, D. H. (2015). Experimental petrology of peridotites, including effects of water and carbon on melting in the Earth's upper mantle. *Physics and Chemistry of Minerals*, *42*(2), 95–122.
Grove, T. L., & Beaty, D. W. (1980). Classification, experimental petrology and possible volcanic histories of the Apollo 11 high-K basalts. *Lunar and Planetary Science Conference Proceedings*, *11*, 149–177.
Grove, T. L., & Bence, A. E. (1977). Experimental study of pyroxene-liquid interaction in quartz-normative basalt 15597. *Lunar and Planetary Science Conference Proceedings*, *8*, 1549–1579.
Grove, T. L., & Bryan, W. B. (1983). Fractionation of pyroxene-phyric MORB at low pressure: An experimental study. *Contributions to Mineralogy and Petrology*, *84*(4), 293–309.
Grove, T. L., Donnelly-Nolan, J. M., & Housh, T. (1997). Magmatic processes that generated the rhyolite of glass mountain, medicine lake volcano, N. California. *Contributions to Mineralogy and Petrology*, *127*(3), 205–223.
Grove, T. L., Gerlach, D. C., & Sando, T. W. (1982). Origin of calc-alkaline series lavas at Medicine Lake volcano by fractionation, assimilation and mixing. *Contributions to Mineralogy and Petrology*, *80*(2), 160–182.

Grove, T. L., & Juster, T. C. (1989). Experimental investigations of low-Ca pyroxene stability and olivine-pyroxene-liquid equilibria at 1-atm in natural basaltic and andesitic liquids. *Contributions to Mineralogy and Petrology*, *103*(3), 287–305.
Grove, T. L., Kinzler, R. J., & Bryan, W. B. (1992). Fractionation of mid-ocean ridge basalt (MORB). *Mantle flow and melt generation at mid-ocean ridges*, *71*, 281–310.
Grove, T. L., & Raudsepp, M. (1978). Effects of kinetics on the crystallization of quartz normative basalt 15597-an experimental study. *Lunar and Planetary Science Conference Proceedings*, *9*, 585–599.
Hart, S. R., & Dunn, T. (1993). Experimental cpx/melt partitioning of 24 trace elements. *Contributions to Mineralogy and Petrology*, *113*(1), 1–8.
Hess, P. C., Rutherford, M. J., & Campbell, H. W. (1978). Ilmenite crystallization in nonmare basalt-genesis of KREEP and high-Ti mare basalt. *Lunar and Planetary Science Conference Proceedings*, *9*, 705–724.
Hesse, M., & Grove, T. L. (2003). Absarokites from the Western Mexican volcanic belt: Constraints on mantle wedge conditions. *Contributions to Mineralogy and Petrology*, *146*(1), 10–27.
Hirschmann, M. M., Kogiso, T., Baker, M. B., & Stolper, E. M. (2003). Alkalic magmas generated by partial melting of garnet pyroxenite. *Geology*, *31*(6), 481–484.
Holbig, E. S., & Grove, T. L. (2008). Mantle melting beneath the Tibetan Plateau: Experimental constraints on ultrapotassic magmatism. *Journal of Geophysical Research*, *113*(B4).
Huang, F., Lundstrom, C. C., & McDonough, W. F. (2006). Effect of melt structure on trace-element partitioning between clinopyroxene and silicic, alkaline, aluminous melts. *American Mineralogist*, *91*(8–9), 1385–1400.
Husen, A., Almeev, R. R., & Holtz, F. (2016). The effect of H_2O and pressure on multiple saturation and liquid lines of descent in basalt from the Shatsky Rise. *Journal of Petrology*, *57*(2), 309–344.
Marziano, G. I., Gaillard, F., & Pichavant, M. (2008). Limestone assimilation by basaltic magmas: An experimental re-assessment and application to Italian volcanoes. *Contributions to Mineralogy and Petrology*, *155*(6), 719–738.
Johnson, K. T. (1998). Experimental determination of partition coefficients for rare Earth and high-field-strength elements between clinopyroxene, garnet, and basaltic melt at high pressures. *Contributions to Mineralogy and Petrology*, *133*(1), 60–68.
Johnston, A. D. (1986). Anhydrous PT phase relations of near-primary high-alumina basalt from the South Sandwich Islands. *Contributions to Mineralogy and Petrology*, *92*(3), 368–382.
Jurewicz, A. J. G., Mittlefehldt, D. W., & Jones, J. H. (1993). Experimental partial melting of the Allende (CV) and Murchison (CM) chondrites and the origin of asteroidal basalts. *Geochimica et Cosmochimica Acta*, *57*(9), 2123–2139.
Jurewicz, A. J. G., Mittlefehldt, D. W., & Jones, J. H. (1995). Experimental partial melting of the st. Severin (LL) and lost city (H) chondrites. *Geochimica et Cosmochimica Acta*, *59*(2), 391–408.
Juster, T. C., Grove, T. L., & Perfit, M. R. (1989). Experimental constraints on the generation of FeTi basalts, andesites, and rhyodacites at the Galapagos Spreading Center, 85 W and 95 W. *Journal of Geophysical Research*, *94*(B7), 9251–9274.
Kawamoto, T. (1996). Experimental constraints on differentiation and H_2O abundance of calc-alkaline magmas. *Earth and Planetary Science Letters*, *144*(3–4), 577–589.
Kelemen, P. B., Joyce, D. B., Webster, J. D., & Holloway, J. R. (1990). Reaction between ultramafic rock and fractionating basaltic magma II. Experimental investigation of reaction between olivine tholeiite and harzburgite at 1150–1050 C and 5 kb. *Journal of Petrology*, *31*(1), 99–134.
Kennedy, A. K., Grove, T. L., & Johnson, R. W. (1990). Experimental and major element constraints on the evolution of lavas from Lihir Island, Papua New Guinea. *Contributions to Mineralogy and Petrology*, *104*(6), 722–734.
Keshav, S., Gudfinnsson, G. H., Sen, G., & Fei, Y. (2004). High-pressure melting experiments on garnet clinopyroxenite and the alkalic to tholeiitic transition in ocean-island basalts. *Earth and Planetary Science Letters*, *223*(3–4), 365–379.
Kinzler, R. J. (1997). Melting of mantle peridotite at pressures approaching the spinel to garnet transition: Application to mid-ocean ridge basalt petrogenesis. *Journal of Geophysical Research*, *102*(B1), 853–874.
Kinzler, R. J., & Grove, T. L. (1985). Crystallization and differentiation of archean komatiite lavas from northeast Ontario: Phase equilibrium and kinetic studies. *American Mineralogist*, *70*(1–2), 40–51.
Kinzler, R. J., & Grove, T. L. (1992). Primary magmas of mid-ocean ridge basalts 1. Experiments and methods. *Journal of Geophysical Research*, *97*(B5), 6885–6906.
Kjarsgaard, B. A. (1998). Phase relations of a carbonated high-CaO nephelinite at 0.2 and 0.5 GPa. *Journal of Petrology*, *39*(11–12), 2061–2075.
Koester, E., Pawley, A. R., Fernandes, L. A., Porcher, C. C., & Soliani, E., Jr. (2002). Experimental melting of cordierite gneiss and the petrogenesis of syntranscurrent peraluminous granites in southern Brazil. *Journal of Petrology*, *43*(8), 1595–1616.
Kägi, R., Müntener, O., Ulmer, P., & Ottolini, L. (2005). Piston-cylinder experiments on H2O undersaturated Fe-bearing systems: An experimental setup approaching f O_2 conditions of natural calc-alkaline magmas. *American Mineralogist*, *90*(4), 708–717.
Kogiso, T., Hirose, K., & Takahashi, E. (1998). Melting experiments on homogeneous mixtures of peridotite and basalt: Application to the Genesis of ocean island basalts. *Earth and Planetary Science Letters*, *162*(1–4), 45–61.
Kogiso, T., & Hirschmann, M. M. (2001). Experimental study of clinopyroxenite partial melting and the origin of ultra-calcic melt inclusions. *Contributions to Mineralogy and Petrology*, *142*(3), 347–360.
Kogiso, T., Hirschmann, M. M., & Frost, D. J. (2003). High-pressure partial melting of garnet pyroxenite: Possible mafic lithologies in the source of ocean island basalts. *Earth and Planetary Science Letters*, *216*(4), 603–617.
Krawczynski, M. J., Grove, T. L., & Behrens, H. (2012). Amphibole stability in primitive arc magmas: Effects of temperature, H_2O content, and oxygen fugacity. *Contributions to Mineralogy and Petrology*, *164*(2), 317–339.
Laporte, D., Toplis, M. J., Seyler, M., & Devidal, J. L. (2004). A new experimental technique for extracting liquids from peridotite at very low degrees of melting: Application to partial melting of depleted peridotite. *Contributions to Mineralogy and Petrology*, *146*(4), 463–484.
Liu, T. C., Chen, B. R., & Chen, C. H. (1998). Anhydrous melting experiment of a Wannienta basalt in the Kuanyinshan area, northern Taiwan, at atmospheric pressure. *Terrestrial, Atmospheric and Oceanic Sciences*, *9*, 165–182.
Liu, T. C., Chen, B. R., & Chen, C. H. (2000). Melting experiment of a Wannienta basalt in the Kuanyinshan area, northern Taiwan, at pressures up to 2.0 GPa. *Journal of Asian Earth Sciences*, *18*(5), 519–531.
Lofgren, G. E., Huss, G. R., & Wasserburg, G. J. (2006). An experimental study of trace-element partitioning between Ti-Al-clinopyroxene and melt: Equilibrium and kinetic effects including sector zoning. *American Mineralogist*, *91*(10), 1596–1606.
Longhi, J. (1995). Liquidus equilibria of some primary lunar and terrestrial melts in the garnet stability field. *Geochimica et Cosmochimica Acta*, *59*(11), 2375–2386.
Longhi, J. (2002). Some phase equilibrium systematics of lherzolite melting: I. *Geochemistry, Geophysics, Geosystems*, *3*(3), 1–33.
Longhi, J., & Pan, V. (1988). A reconnaisance study of phase boundaries in low-alkali basaltic liquids. *Journal of Petrology*, *29*(1), 115–147.
Longhi, J., & Pan, V. (1989). The parent magmas of the SNC meteorites. *Lunar and Planetary Science Conference Proceedings*, *19*, 451–464.

Ma, S., & Shaw, C. S. (2021). An experimental study of trace element partitioning between peridotite minerals and alkaline basaltic melts at 1250°C and 1 GPa: Crystal and melt composition impacts on partition coefficients. *Journal of Petrology*, *62*(11), egab084.
Maaløe, S. (2004). The solidus of harzburgite to 3 GPa pressure: The compositions of primary abyssal tholeiite. *Mineralogy and Petrology*, *81*(1–2), 1–17.
Mahood, G. A., & Baker, D. R. (1986). Experimental constraints on depths of fractionation of mildly alkalic basalts and associated felsic rocks: Pantelleria, Strait of Sicily. *Contributions to Mineralogy and Petrology*, *93*(2), 251–264.
Martel, C., Champallier, R., Prouteau, G., Pichavant, M., Arbaret, L., Balcone-Boissard, H., et al. (2013). Trachyte phase relations and implication for magma storage conditions in the Chaîne des Puys (French Massif Central). *Journal of Petrology*, *54*(6), 1071–1107.
Martel, C., Pichavant, M., Holtz, F., Scaillet, B., Bourdier, J. L., & Traineau, H. (1999). Effects of f O_2 and H_2O on andesite phase relations between 2 and 4 kbar. *Journal of Geophysical Research*, *104*(B12), 29453–29470.
Masotta, M., Freda, C., & Gaeta, M. (2012). Origin of crystal-poor, differentiated magmas: Insights from thermal gradient experiments. *Contributions to Mineralogy and Petrology*, *163*(1), 49–65.
McCoy, T. J., & Lofgren, G. E. (1999). Crystallization of the Zagami shergottite: An experimental study. *Earth and Planetary Science Letters*, *173*(4), 397–411.
McDade, P., Blundy, J. D., & Wood, B. J. (2003). Trace element partitioning on the Tinaquillo Lherzolite solidus at 1.5 GPa. *Physics of the Earth and Planetary Interiors*, *139*(1–2), 129–147.
McKay, G., Wagstaff, J., & Yang, S. R. (1986). Clinopyroxene REE distribution coefficients for shergottites: The REE content of the Shergotty melt. *Geochimica et Cosmochimica Acta*, *50*(6), 927–937.
Médard, E., & Grove, T. L. (2008). The effect of H 2 O on the olivine liquidus of basaltic melts: Experiments and thermodynamic models. *Contributions to Mineralogy and Petrology*, *155*(4), 417–432.
Medard, E., Schmidt, M. W., & Schiano, P. (2004). Liquidus surfaces of ultracalcic primitive melts: Formation conditions and sources. *Contributions to Mineralogy and Petrology*, *148*(2), 201–215.
Meen, J. K. (1987). Formation of shoshonites from calcalkaline basalt magmas: Geochemical and experimental constraints from the type locality. *Contributions to Mineralogy and Petrology*, *97*(3), 333–351.
Meen, J. K. (1990). Elevation of potassium content of basaltic magma by fractional crystallization: The effect of pressure. *Contributions to Mineralogy and Petrology*, *104*(3), 309–331.
Melekhova, E., Blundy, J., Martin, R., Arculus, R., & Pichavant, M. (2017). Petrological and experimental evidence for differentiation of water-rich magmas beneath St. Kitts, Lesser Antilles. *Contributions to Mineralogy and Petrology*, *172*(11), 1–32.
Melekhova, E., Blundy, J., Robertson, R., & Humphreys, M. C. (2015). Experimental evidence for polybaric differentiation of primitive arc basalt beneath St. Vincent, Lesser Antilles. *Journal of Petrology*, *56*(1), 161–192.
Mengel, K., & Green, D. H. (1986). Experimental study of amphibole and phlogopite stability in metasomatized peridotite under water-saturated and water-undersaturated conditions. *International kimberlite conference: extended abstracts*, *4*, 193–195.
Müntener, O., Kelemen, P. B., & Grove, T. L. (2001). The role of H_2O during crystallization of primitive arc magmas under uppermost mantle conditions and Genesis of igneous pyroxenites: An experimental study. *Contributions to Mineralogy and Petrology*, *141*(6), 643–658.
Mercer, C. N., & Johnston, A. D. (2008). Experimental studies of the P–T–H_2O near-liquidus phase relations of basaltic andesite from north sister volcano, high Oregon cascades: Constraints on lower-crustal mineral assemblages. *Contributions to Mineralogy and Petrology*, *155*(5), 571–592.
Minitti, M. E., & Rutherford, M. J. (2000). Genesis of the Mars Pathfinder "sulfur-free" rock from SNC parental liquids. *Geochimica et Cosmochimica Acta*, *64*(14), 2535–2547.
Mollo, S., Del Gaudio, P., Ventura, G., Iezzi, G., & Scarlato, P. (2010). Dependence of clinopyroxene composition on cooling rate in basaltic magmas: Implications for thermobarometry. *Lithos*, *118*(3–4), 302–312.
Mollo, S., Gaeta, M., Freda, C., Di Rocco, T., Misiti, V., & Scarlato, P. (2010). Carbonate assimilation in magmas: A reappraisal based on experimental petrology. *Lithos*, *114*(3–4), 503–514.
Mollo, S., Forni, F., Bachmann, O., Blundy, J. D., De Astis, G., & Scarlato, P. (2016). Trace element partitioning between clinopyroxene and trachy-phonolitic melts: A case study from the campanian ignimbrite (campi flegrei, Italy). *Lithos*, *252*, 160–172.
Mollo, S., Putirka, K., Misiti, V., Soligo, M., & Scarlato, P. (2013). A new test for equilibrium based on clinopyroxene–melt pairs: Clues on the solidification temperatures of Etnean alkaline melts at post-eruptive conditions. *Chemical Geology*, *352*, 92–100.
Moore, G., & Carmichael, I. S. E. (1998). The hydrous phase equilibria (to 3 kbar) of an andesite and basaltic andesite from Western Mexico: Constraints on water content and conditions of phenocryst growth. *Contributions to Mineralogy and Petrology*, *130*(3), 304–319.
Moriyama, J., Kawabe, I., Fujino, K., & Ohtani, E. (1992). Experimental study of element partitioning between majorite, olivine, merwinite, diopside and silicate melts at 16 GPa and 2, 000°C. *Geochemical Journal*, *26*(6), 357–382.
Nandedkar, R. H., Ulmer, P., & Müntener, O. (2014). Fractional crystallization of primitive, hydrous arc magmas: An experimental study at 0.7 GPa. *Contributions to Mineralogy and Petrology*, *167*(6), 1–27.
Naney, M. T. (1983). Phase equilibrium of rock-forming ferromagnesian silicates in granitic systems. *American Journal of Science*, *283*, 993–1033.
Nekvasil, H., Dondolini, A., Horn, J., Filiberto, J., Long, H., & Lindsley, D. H. (2004). The origin and evolution of silica-saturated alkalic suites: An experimental study. *Journal of Petrology*, *45*(4), 693–721.
Parat, F., Streck, M. J., Holtz, F., & Almeev, R. (2014). Experimental study into the petrogenesis of crystal-rich basaltic to andesitic magmas at Arenal volcano. *Contributions to Mineralogy and Petrology*, *168*(2), 1040.
Parman, S. W., Dann, J. C., Grove, T. L., & De Wit, M. J. (1997). Emplacement conditions of komatiite magmas from the 3.49 Ga Komati Formation, Barberton greenstone belt, South Africa. *Earth and Planetary Science Letters*, *150*(3–4), 303–323.
Parman, S. W., & Grove, T. L. (2004). Harzburgite melting with and without H_2O: Experimental data and predictive modeling. *Journal of Geophysical Research*, *109*(B2).
Patiño Douce, A. E. (1995). Experimental generation of hybrid silicic melts by reaction of high-Al basalt with metamorphic rocks. *Journal of Geophysical Research*, *100*(B8), 15623–15639.
Patiño Douce, A. E. (2005). Vapor-absent melting of tonalite at 15–32 kbar. *Journal of Petrology*, *46*(2), 275–290.
Patiño Douce, A. E., & Beard, J. S. (1995). Dehydration-melting of biotite gneiss and quartz amphibolite from 3 to 15 kbar. *Journal of Petrology*, *36*(3), 707–738.
Pertermann, M., & Lundstrom, C. C. (2006). Phase equilibrium experiments at 0.5 GPa and 1100–1300 C on a basaltic andesite from Arenal volcano, Costa Rica. *Journal of Volcanology and Geothermal Research*, *157*(1–3), 222–235.
Pichavant, M., Martel, C., Bourdier, J. L., & Scaillet, B. (2002). Physical conditions, structure, and dynamics of a zoned magma chamber: Mount Pelée (Martinique, Lesser Antilles Arc). *Journal of Geophysical Research*, *107*(B5), ECV-1.

Pichavant, M., Mysen, B. O., & Macdonald, R. (2002). Source and H_2O content of high-MgO magmas in island arc settings: An experimental study of a primitive calc-alkaline basalt from st. Vincent, lesser antilles arc. *Geochimica et Cosmochimica Acta*, *66*(12), 2193–2209.
Pichavant, M., Poussineau, S., Lesne, P., Solaro, C., & Bourdier, J. L. (2018). Experimental parametrization of magma mixing: Application to the AD 1530 eruption of La soufrière, Guadeloupe (lesser antilles). *Journal of Petrology*, *59*(2), 257–282.
Pickering-Witter, J., & Johnston, A. D. (2000). The effects of variable bulk composition on the melting systematics of fertile peridotitic assemblages. *Contributions to Mineralogy and Petrology*, *140*(2), 190–211.
Pietranik, A., Holtz, F., Koepke, J., & Puziewicz, J. (2009). Crystallization of quartz dioritic magmas at 2 and 1 kbar: Experimental results. *Mineralogy and Petrology*, *97*(1–2), 1.
Prouteau, G., & Scaillet, B. (2003). Experimental constraints on the origin of the 1991 Pinatubo dacite. *Journal of Petrology*, *44*(12), 2203–2241.
Putirka, K., Johnson, M., Kinzler, R., Longhi, J., & Walker, D. (1996). Thermobarometry of mafic igneous rocks based on clinopyroxene-liquid equilibria, 0–30 kbar. *Contributions to Mineralogy and Petrology*, *123*(1), 92–108.
Putirka, K. D., Mikaelian, H., Ryerson, F., & Shaw, H. (2003). New clinopyroxene-liquid thermobarometers for mafic, evolved, and volatile-bearing lava compositions, with applications to lavas from Tibet and the Snake River Plain, Idaho. *American Mineralogist*, *88*(10), 1542–1554.
Rhodes, J. M., Lofgren, G. E., & Smith, D. P. (1979). One atmosphere melting experiments on ilmenite basalt 12008. *Lunar and Planetary Science Conference Proceedings*, *10*, 407–422.
Robinson, J. A. C., Wood, B. J., & Blundy, J. D. (1998). The beginning of melting of fertile and depleted peridotite at 1.5 GPa. *Earth and Planetary Science Letters*, *155*(1–2), 97–111.
Rushmer, T. (1993). Experimental high-pressure granulites: Some applications to natural mafic xenolith suites and Archean granulite terranes. *Geology*, *21*(5), 411–414.
Sack, R. O., Walker, D., & Carmichael, I. S. (1987). Experimental petrology of alkalic lavas: Constraints on cotectics of multiple saturation in natural basic liquids. *Contributions to Mineralogy and Petrology*, *96*(1), 1–23.
Salters, V. J., & Longhi, J. (1999). Trace element partitioning during the initial stages of melting beneath mid-ocean ridges. *Earth and Planetary Science Letters*, *166*(1–2), 15–30.
Scaillet, B., & Macdonald, R. A. Y. (2003). Experimental constraints on the relationships between peralkaline rhyolites of the Kenya Rift Valley. *Journal of Petrology*, *44*(10), 1867–1894.
Schmidt, M. W., Green, D. H., & Hibberson, W. O. (2004). Ultra-calcic magmas generated from Ca-depleted mantle: An experimental study on the origin of ankaramites. *Journal of Petrology*, *45*(3), 531–554.
Schwab, B. E., & Johnston, A. D. (2001). Melting systematics of modally variable, compositionally intermediate peridotites and the effects of mineral fertility. *Journal of Petrology*, *42*(10), 1789–1811.
Scoates, J. S., Cascio, M. L., Weis, D., & Lindsley, D. H. (2006). Experimental constraints on the origin and evolution of mildly alkalic basalts from the Kerguelen Archipelago, Southeast Indian Ocean. *Contributions to Mineralogy and Petrology*, *151*(5), 582–599.
Sisson, T. W., & Grove, T. L. (1993). Experimental investigations of the role of H_2O in calc-alkaline differentiation and subduction zone magmatism. *Contributions to Mineralogy and Petrology*, *113*(2), 143–166.
Skjerlie, K. P., & Johnston, A. D. (1996). Vapour-absent melting from 10 to 20 kbar of crustal rocks that contain multiple hydrous phases: Implications for anatexis in the deep to very deep continental crust and active continental margins. *Journal of Petrology*, *37*(3), 661–691.
Skjerlie, K. P., & Patiño Douce, A. E. (2002). The fluid-absent partial melting of a zoisite-bearing quartz eclogite from 1·0 to 3·2 GPa; implications for melting in thickened continental crust and for subduction-zone processes. *Journal of Petrology*, *43*(2), 291–314.
Skulski, T., Minarik, W., & Watson, E. B. (1994). High-pressure experimental trace-element partitioning between clinopyroxene and basaltic melts. *Chemical Geology*, *117*(1–4), 127–147.
Spandler, C., Yaxley, G., Green, D. H., & Rosenthal, A. (2008). Phase relations and melting of anhydrous K-bearing eclogite from 1200 to 1600 C and 3 to 5 GPa. *Journal of Petrology*, *49*(4), 771–795.
Springer, W., & Seck, H. A. (1997). Partial fusion of basic granulites at 5 to 15 kbar: Implications for the origin of TTG magmas. *Contributions to Mineralogy and Petrology*, *127*(1–2), 30–45.
Stolper, E. (1977). Experimental petrology of eucritic meteorites. *Geochimica et Cosmochimica Acta*, *41*(5), 587–611.
Stolper, E. (1980). A phase diagram for mid-ocean ridge basalts: Preliminary results and implications for petrogenesis. *Contributions to Mineralogy and Petrology*, *74*(1), 13–27.
Takagi, D., Sato, H., kagawa, N., Takagi, D., Sato, H., & Nakagawa, M. (2005). Experimental study of a low-alkali tholeiite at 1–5 kbar: Optimal condition for the crystallization of high-an plagioclase in hydrous arc tholeiite. *Contributions to Mineralogy and Petrology*, *149*(5), 527–540.
Takahashi, E. (1980). Thermal history of iherzolite xenoliths—I. Petrology of iherzolite xenoliths from the ichinomegata crater, oga peninsula, northeast Japan. *Geochimica et Cosmochimica Acta*, *44*(11), 1643–1658.
Takahahshi, E., Nakajima, K., & Wright, T. L. (1998). Origin of the columbia river basalts: Melting model of a heterogeneous plume head. *Earth and Planetary Science Letters*, *162*(1–4), 63–80.
Thy, P., Lesher, C. E., & Fram, M. S. (1998). Low pressure experimental constraints on the evolution of basaltic lavas from Site 917, southeast Greenland continental margin. *Proceedings of Ocean Drilling Program scientific Results*, *152*, 359–372.
Thy, P., Lesher, C. E., Nielsen, T. F. D., & Brooks, C. K. (2006). Experimental constraints on the Skaergaard liquid line of descent. *Lithos*, *92*(1–2), 154–180.
Toplis, M. J., & Carroll, M. R. (1995). An experimental study of the influence of oxygen fugacity on Fe-Ti oxide stability, phase relations, and mineral—Melt equilibria in ferro-basaltic systems. *Journal of Petrology*, *36*(5), 1137–1170.
Tormey, D. R., Grove, T. L., & Bryan, W. B. (1987). Experimental petrology of normal MORB near the kane fracture zone: 22–25 N, mid-atlantic ridge. *Contributions to Mineralogy and Petrology*, *96*(2), 121–139.
Tsuruta, K., & Takahashi, E. (1998). Melting study of an alkali basalt JB-1 up to 12.5 GPa: Behavior of potassium in the deep mantle. *Physics of the Earth and Planetary Interiors*, *107*(1–3), 119–130.
Tuff, J., Takahashi, E., & Gibson, S. A. (2005). Experimental constraints on the role of garnet pyroxenite in the Genesis of high-Fe mantle plume derived melts. *Journal of Petrology*, *46*(10), 2023–2058.
Ulmer, P., Kaegi, R., & Müntener, O. (2018). Experimentally derived intermediate to silica-rich arc magmas by fractional and equilibrium crystallization at 1·0 GPa: An evaluation of phase relationships, compositions, liquid lines of descent and oxygen fugacity. *Journal of Petrology*, *59*(1), 11–58.
Ulmer, P., & Sweeney, R. J. (2002). Generation and differentiation of group II kimberlites: Constraints from a high-pressure experimental study to 10 GPa. *Geochimica et Cosmochimica Acta*, *66*(12), 2139–2153.

Vander Auwera, J., & Longhi, J. (1994). Experimental study of a jotunite (hypersthene monzodiorite): Constraints on the parent magma composition and crystallization conditions (P, T, f O_2) of the bjerkreim-sokndal layered intrusion (Norway). *Contributions to Mineralogy and Petrology*, *118*(1), 60–78.

Vander Auwera, J., Longhi, J., & Duchesne, J. C. (1998). A liquid line of descent of the jotunite (hypersthene monzodiorite) suite. *Journal of Petrology*, *39*(3), 439–468.

Villiger, S., Ulmer, P., & Müntener, O. (2007). Equilibrium and fractional crystallization experiments at 0·7 GPa; the effect of pressure on phase relations and liquid compositions of tholeiitic magmas. *Journal of Petrology*, *48*(1), 159–184.

Villiger, S., Ulmer, P., Müntener, O., & Thompson, A. B. (2004). The liquid line of descent of anhydrous, mantle-derived, tholeiitic liquids by fractional and equilibrium crystallization—An experimental study at 1·0 GPa. *Journal of Petrology*, *45*(12), 2369–2388.

Wagner, T. P., & Grove, T. L. (1998). Melt/harzburgite reaction in the petrogenesis of tholeiitic magma from Kilauea volcano, Hawaii. *Contributions to Mineralogy and Petrology*, *131*(1), 1–12.

Walter, M. J. (1998). Melting of garnet peridotite and the origin of komatiite and depleted lithosphere. *Journal of Petrology*, *39*(1), 29–60.

Wang, W., & Takahashi, E. (1999). Subsolidus and melting experiments of a K-rich basaltic composition to 27 GPa: Implication for the behavior of potassium in the mantle. *American Mineralogist*, *84*(3), 357–361.

Wasylenki, L. E., Baker, M. B., Kent, A. J., & Stolper, E. M. (2003). Near-solidus melting of the shallow upper mantle: Partial melting experiments on depleted peridotite. *Journal of Petrology*, *44*(7), 1163–1191.

Whitaker, M. L., Nekvasil, H., Lindsley, D. H., & Difrancesco, N. J. (2007). The role of pressure in producing compositional diversity in intraplate basaltic magmas. *Journal of Petrology*, *48*(2), 365–393.

Whitaker, M. L., Nekvasil, H., Lindsley, D. H., & McCurry, M. (2008). Can crystallization of olivine tholeiite give rise to potassic rhyolites?—An experimental investigation. *Bulletin of Volcanology*, *70*(3), 417–434.

Wood, B. J., & Trigila, R. (2001). Experimental determination of aluminous clinopyroxene–melt partition coefficients for potassic liquids, with application to the evolution of the Roman province potassic magmas. *Chemical Geology*, *172*(3–4), 213–223.

Yang, H. J., Kinzler, R. J., & Grove, T. L. (1996). Experiments and models of anhydrous, basaltic olivine-plagioclase-augite saturated melts from 0.001 to 10 kbar. *Contributions to Mineralogy and Petrology*, *124*(1), 1–18.

Yasuda, A., Fujii, T., & Kurita, K. (1994). Melting phase relations of an anhydrous mid-ocean ridge basalt from 3 to 20 GPa: Implications for the behavior of subducted oceanic crust in the mantle. *Journal of Geophysical Research*, *99*(B5), 9401–9414.

Zhang, R. Y., Zhai, S. M., Fei, Y. W., & Liou, J. G. (2003). Titanium solubility in coexisting garnet and clinopyroxene at very high pressure: The significance of exsolved rutile in garnet. *Earth and Planetary Science Letters*, *216*(4), 591–601.